# ODD-ELECTRONS APPROACH TO COVALENT CHEMISTRY AND MAGNETISM OF SINGLE-WALL CARBON NANOTUBES AND GRAPHENE

E.F. Sheka* and L.A. Chernozatonskii**

** Peoples' Friendship University of Russia, Moscow*
*** Emanuel Institute of Biochemical Physics, RAS, Moscow*

sheka@icp.ac.ru

Received 29.04.2009

The covalent chemistry and magnetism of single-walled carbon nanotubes and graphene is considered on the basis of peculiarities of odd electron interaction in the studied nanocarbons. The term indicates that the number of valence electrons of each nanocarbon atom is larger by one than the number of chemical bonds it forms. The main issue of the odd-electron concept concerns a partly radical character of the species which is resulted from the presence of *effectively unpaired electrons* that constitute a part of odd electrons excluded from the covalent bonding. The total number of effectively unpaired electrons $N_D$ and its fraction on each atom $N_{DA}$ are suggested as quantifiers of molecular atomic susceptibility and atomic chemical susceptibility, respectively, thus highlighting targets that are the most favorable for addition reactions of any type. The approach is illustrated for two families of carbon nanotubes involving fragments of arm-chair (n,n) and zigzag (m,0) single-walled nanotubes different by the length and end structure, as well as by a set of nanographenes and silicene. Simultaneously, the odd-electron concept lays the foundation for exhibiting the magnetism when nanostructuring of the species provides a significant weakening of the electron interaction so that exchange integrals, describing exchange electron interaction, become small enough to favor magnetic ordering in the body. The suggested "scaly" nature of the phenomenon is well consistent with the latest experimental findings.

УДК 539.19, 544.1, 546.26

## 1. Introduction

Fullerenes, carbon nanotubes, graphene, and some other nanostructured carboneous materials take a particular place among molecular species with odd electrons. The term was introduced in organic chemistry when describing the electronic structure of diradicals [1, 2] and naturally covers terming “magnetic electrons” [3] as well as “open-shell molecule electrons’ [4]. Concerning carbon nanotubes and graphene, it manifests that the number of valence electrons of each atom of the nanocarbons is larger by one than that of interatomic bonds the atom forms. Each pair of carbon atoms of the species possesses two such electrons, similarly to, say, ethylene and benzene molecules. But oppositely to the latter, the interaction between the electrons is much weaker. The finding is resulted from a considerable enlarging

of the C-C distances [5]. The approach generalization for systems with weak coupling that causes the appearance of nearly degenerate spin states ultimately requires taking into account the electron correlation and passing to computational schemes that involve full configurational interaction (CI). However, the traditional complete-active-space-self-consistent-field (CASSCF) methods that deal correctly with two-odd electrons systems such as diradicals and some dinuclear magnetic complexes (see comprehensive review [6]), cannot handle systems with larger number of odd electrons due to a huge number of configurations generated in the active space of the system. To imagine arising severe technical difficulties it is worthwhile to cite [6], "If there are '*m*' singly occupied orbitals on each of '*n*' identical centers, then $2^{mn}$ Slater determinants can be formed by assigning spins up or down each of the '*nm*' orbitals". So that no CASSCF type approach, including a simplified embedded-cluster CASSCF supplemented by the complete active space second-order perturbation theory (CASPT2) [7], seems feasible for many-odd electron systems such as fullerenes, carbon nanotubes, and graphene. That is why addressing the single-determinant approaches seems to be the only alternative.

The open-shell unrestricted broken spin-symmetry (UBS) approach suggested by Noodleman [8] is the most widely known among the latter. The approach is well elaborated for both wave-function (Ψ-based) and electron-density (ρ-based) quantum-chemical methodologies, followed from the unrestricted single-determinant Hartree-Fock scheme [9] and spin-dependent local-spin-density-approximated (LSDA) density-functional theory (DFT) that, in its turn, is based on the Kohn-Sham single Slater determinant procedure [10]. In what follows we shall refer to them as UBS HF and UBS DFT, respectively.

The main problem of the UBS approach concerns spin-contamination of the calculation results. The contamination contribution depends on the interaction between the odd electrons and increases considerably when the interaction decreases. However, if this evident fact is willingly accepted for UBS HF and is often addressed as the approach disadvantage, a widely spread illusion exists that the spin-polarized DFT approach provides obtaining pure spin states. In reality, as shown in [11], it is not so and the DFT solution that is UBS in reality is spin-contaminated as well due to single-determinant character of the wave functions that form the electron density. Ignoring this fact leads to wrong conclusions such as the prediction of unreal magnetic properties of graphene ribbons (see the detailed discussion of the problem in [12]).

The problem presents difficulties in the interpretation of UBS results in view of their relevance to physical and chemical reality that consists in mapping between the eigenvalues and eigenfunctions of exact and model spin Hamiltonians. While the implementation of UBS HF approach, both *ab initio* and semiempirical, is quite unique and the desired mapping is quite straightforward, this cannot be said about calculation schemes based on LSDA DFT [4]. This is caused by a fundamental problem of DFT concerning the total spin. For long ago has it been known that DFT cannot be directly applied to the calculation of the spin and space multiplet structure (a comprehensive analysis of problems existing in the present formulation of DFT is performed in [13]). A number of special procedures, that all are beyond the pure DFT scope [14], were suggested to overcome the difficulty. The procedures differ by computation schemes as well as by the obtained results so that UBS DFT is method-dependent [4, 13-15]. This greatly complicates the comparison of the data obtained by different computational versions and poses severe obstacles in computational experiments aimed at obtaining quantitative-structure-activity-relationships attaching them to a particular computational scheme, therewith without being absolutely sure about the result reliability. This is one reason why the preference of UBS HF is obvious if the relationships of this kind are the main goal of the study. The other reason is connected with complete theoretical transparency of UBS HF scheme when any quantity, including total spin, has a clear physical meaning and a proper description. However, it should be kept in mind that UBS HF is only an

approximation to the exact solution so that a thorough analysis should be made connecting the obtained results with physical or chemical reality. Fortunately, there is a well elaborated way providing such mapping which will be discussed in the next Section.

The current review exhibits a platform for the UBS HF application to disclosing quantitative-structure-activity-relationships related to single-walled carbon nanotubes (SWCARBON NANOTUBEs) and graphene. A large set of fragments related to armchair (n,n) and zigzag (m,0) SWCARBON NANOTUBEs different by length and end structure, namely, short and long as well as those with end caps and open ends, in the latter case, both hydrogen terminated and empty ones are discussed. The main result concerns exhibiting quantified chemical susceptibility (or equivalently, reactivity) of the tube atoms that allowed dividing the tubes space into a small number of characteristic regions related to differently configured ends, sidewall and defects. The finding allowed suggesting a unique algorithm for the quantitative description of the atomically matched chemical susceptibility of SWCARBON NANOTUBEs of any length and any end composition and gave a clear vision for experimentalists and engineers how to proceed with the chemical covalent functionalization of SWCARBON NANOTUBEs aiming at obtaining desired chemical compositions. Similar description of graphene highlighted main peculiarities of its chemical behavior and showed the way of explaining magnetic properties of the species. A detailed description of silicon-based counterparts of SWCARBON NANOTUBEs and graphene completes the review.

## 2. Broken Spin-Symmetry Approach

### 2.1. Odd-electron-enhanced chemical reactivity

UBS HF and UBS DFT find favor over close-shell computational schemes because the "correlation effects" by Löwdin [16] are automatically introduced at least through different-orbital-different-spin understanding. Both starting approaches, UHF and LSDA correspond to the state with the definite value of the spin projection $S_z$, but does not, in general, correspond to the state with the definite value of the total spin S, so that

$$\hat{S}_z\psi^{UHF} = S_z\psi^{UHF} \text{ and } \hat{S}_z\psi^{LSDA} = S_z\psi^{LSDA}$$

$$\text{but } \hat{S}^2\ \psi^{UHF} \neq S(S+1)\psi^{UHF} \text{ and } \hat{S}^2\ \psi^{LSDA} \neq S(S+1)\psi^{LSDA}. \quad (1)$$

As a result, both solutions are spin-contaminated if only all electron spins are either not coupled which leads to S=0 or have not one direction so that $S=S_{max}$. The contamination

$$C = \left\langle \hat{S}^2 \right\rangle - S(S+1) \quad (2)$$

is often substantial.

The inequalities in (1) result in the Löwdin symmetry dilemma [17] that is expressed as asymmetric electron densities of UBS HF solution and asymmetric LSDA Hamiltonian of UBS DFT with different exchange-correlation potentials for spin-up and spin-down orbitals. The asymmetry produces the appearance of spin density in the general form [18] (see the latest discussion of the problem in [6, 19])

$$D(r|r') = 2\rho(r|r') - \int \rho(r|r'')\rho(r''|r')dr''. \quad (3)$$

In the case of the UBS HF approach $D(r|r')$ is determined as

$$DS = 2PS - (PS)^2 \quad (4)$$

Here $P = P^{\alpha} + P^{\beta}$ is the density matrix and $S$ is the orbital overlap matrix (α and β mark different spin directions). If the UBS HF computations are realized via *NDDO* approximation (the basis for AM1/PM3 versions of semiempirical techniques), a zero overlap of orbitals results in $S = I$, where $I$ is the identity matrix. The spin density matrix $D$ then assumes the form [20]

$$D = \left(P^{\alpha} - P^{\beta}\right)^2. \tag{5}$$

The elements of the density matrices $P_{ij}^{\alpha(\beta)}$ can be written in terms of eigenvectors of the UBS HF solution $C_{ik}$

$$P_{ij}^{\alpha(\beta)} = \sum_{k}^{N^{\alpha(\beta)}} C_{ik}^{\alpha(\beta)} * C_{jk}^{\alpha(\beta)}, \tag{6}$$

where $N^{\alpha}$ and $N^{\beta}$ are the numbers of electrons with spins $\alpha$ and $\beta$, respectively. These explicit equations are the consequence of the Ψ-based character of UHF. Since the corresponding coordinate wave functions are subordinated to the definite permutation symmetry, each value of spin $S$ corresponds to a definite expectation value of energy [14].

Oppositely, the electron density ρ is invariant to the permutation symmetry [14]. That is why spin density $D(r|r')$ of UBS DFT depends on spin-dependent exchange and correlation functionals only and cannot be expressed analytically. Since the exchange-correlation composition deviates from one method to the other, the spin density is not fixed and deviates alongside with the composition.

Leaving aside the problem of the pure-spin state extraction from the spin-contaminated unrestricted solutions which is differently complicated for UBS HF and UBS DFT, let us discuss the pragmatic usefulness provided by the UBS solutions. Obviously, spin-contamination $C$ and spin density $D(r|r')$ exhibit incompleteness of taking correlation effects into account. The latter, governed by the Fock exchange only, is evidently the largest which is the case of UBS HF. As for UBS DFT, there are additional possibilities concerning functionals in use: from the Fock exchange the only functional that causes severe underestimation of the correlation effects to local density approximation (LDA) that provides a huge overestimation, so mixing the Fock and LDA exchange can provide any beforehand decided (method-dependent) result [4, 15]. Oppositely to this fact, UBS HF solution is strictly standard. At the same time, the solution retains a transparent single-determinant description, the restricted version of which led the foundation of the modern chemistry language, due to which a question arises if there is a possibility "to translate" the correlation incompleteness of UBS HF in convenient terms so that it will become practically useful if properly designed.

A suggestion to use the correlation incompleteness of the UBS solution for practical goals is usually connected with Noodleman's publication [8]. Since then the term "broken symmetry approach" or "broken spin-symmetry approach" appeared. However, Noodleman's consideration was restricted to obtaining exchange integral $J$ which is directly related to the energy difference of the Heisenberg Hamiltonian eigenstates and is of big importance for considering magnetic properties. The parameter also provides the correct calculation of the energy of pure spin states. However, the first addressing to UBS solution in view of its use for practical chemistry was made earlier [18]. The authors showed that the extra spin density of the UBS solution $D(r|r')$ could be interpreted in terms of *effectively unpaired electrons* that constitute a part of valence electrons withdrawn from the covalent bonding. Within the framework of UBS HF the quantity can be explicitly determined in the form [20]

$$N_{DA} = \sum_{i \in A} \sum_{B=1}^{NAT} \sum_{j \in B} D_{ij} \tag{7}$$

and

$$N_D = \sum_A N_{DA} = \sum_{i,j=1}^{NORBS} D_{ij} , \tag{8}$$

where $N_{DA}$ determines the Effectively unpaired electrons number on atom $A$ while $N_D$ constitutes the total Effectively unpaired electrons number. The summation is performed over a number of atoms in the first case and over all atomic orbitals in the second.

Firstly applied to fullerenes [5, 20], $N_{DA}$ was shown to disclose the chemical activity of individual molecule atoms which was termed as *atomic chemical susceptibility* (ACS). Similarly referred to, $N_D$ can be called *molecular chemical susceptibility* (MCS). Atomically matched $N_{DA}$ is a quantifier thus highlighting targets that are the most favorable for addition reactions of any type. Practical realization of computational synthesis of fullerene $C_{60}$ derivatives proved the great importance of the two quantities in describing chemical reactions and their products.

Oppositely to UBS HF, UBS DFT does not suggest any quantity similar to either $N_D$ or $N_{DA}$. This might be a reason why UBS DFT calculations are rather scarce. The available results concerning UBS DFT calculations of SWCARBON NANOTUBEs and graphene will be discussed in Sections 4.2 and 4.5.

### 2.2. Odd-electron magnetism

Molecular magnetism of odd-electron systems can be considered in terms of the Heisenberg Hamiltonian [21] via the total spin $S$ and the exchange integral $J$ or, as mainly referred to now, the magnetic coupling constant [15]. The eigenfunctions of the Hamiltonian are simply spin eigenfunctions and $J$ is directly related to the energy difference corresponding to these eigenstates. The determination of the magnetic coupling constant is a central point of the magnetism study.

Attempts to apply the Heisenberg description of magnetic interaction to the electronic structure of a molecular electron system have been undertaken by many authors (see reviews [15, 21] and references therein). A successful description of such a delicate physical property lies in the appropriate mapping between the Heisenberg spin eigenstates and the suitable computationally determined electronic states. It is customary to derive the relationship between $J$ and the energy difference of pure-spin states.

As for UBS HF approach where electronic states are definitely spin-mapped, the problem consists in the determination of pure-spin states and the relevant $J$ value from the spin-contaminated eigenvalues of the UBS HF solutions. The problem was perfectly decided by Noodleman [8, 22] within the broken spin-symmetry approach, so that in the case of even number of "magnetic" (odd) electrons $J$ is determined as

$$J = \frac{E_{S=0}^{UBS\ \ HF} - E_{S_{\max}}^{PS}}{S_{\max}^2} . \tag{9}$$

Here $E_{S=0}^{UBS\ \ HF}$ and $E_{S_{\max}}^{PS}$ are the energy of the UBS HF singlet state and the pure-spin state with maximal spin $S_{\max}$ that is the exact pure-spin single-determinant solution, respectively. Consequently, the energy of the pure spin singlet state is determined by the equation [8]

$$E_{S=0}^{PS} = E_{S=0}^{UBS\ \ HF} + S_{\max} J , \tag{10}$$

while the energy of the subsequent pure-spin states of the higher spin multiplicity are determined as

$$E_S^{PS} = E_{S=0}^{PS} - S(S+1)J\,. \qquad (11)$$

As said above, both magnetic coupling constant $J$ and pure-spin states cannot be straightforwardly obtained within the DFT scope. Usually, particular procedures are used to reach the goal. Without pretending to give an exhaustive list of publications concerning the problem some representative examples may be found in Refs. [4, 19, 22-24]. Some of these attempts were rather successful in view of comparison with experimental data that is the case of the long-year studying of magnetic behavior of biomoleculat complexes with transition metals [25].

Magnetism is the phenomenon specified by weak electronic interaction so that the object magnetization proceeds when $J$ absolute value is small. That is of a particular importance for the magnetism appearance in systems with the singlet ground state due to the second-order character of the magnetic phenomenon in this case [26]. At the same time, the $J$ value obviously correlates with the number of effectively unpaired electrons and the UBS spin density $D(r|r')$ that both increase when $J$ decreases. However, there is no exact relation between $J$, on one hand, and either $N_D$ or $D(r|r')$, on the other. That is why the empirically known upper limit of the absolute $J$ value, at which the magnetization of a species starts to be exhibited, at the level of $10^{-2}$-$10^{-3}$ kcal/mol [27] cannot be straightforwardly translated into the corresponding values for $N_D$ or $D(r|r')$. So that $J$ retains the only quantity that may quantify the magnetic behavior from the theoretical viewpoint. The $J$-approach to magnetism consideration concerning nanocarbons was firstly applied to polymerized crystalline fullerene $C_{60}$ [28]. In the current review similar approach is applied to nanographenes (see Section 5).

## 3. Diatomic Molecules

The analysis of the $N_D$ values behavior along the potential energy curve of diatomic molecules gives an excellent possibility to check the correctness of the UBS HF approach to the description of effectively unpaired electrons. The calculations were performed for hydrogen, nitrogen, and oxygen molecules [5, 20, 29]. The obtained data for the ground states of molecules (singlet $H_2$ and $N_2$, and triplet $O_2$) are plotted in Fig. 1. As seen from the figure, a characteristic $S$-like character of the $N_D(R)$ dependencies is common for all molecules. Each $N_D(R)$ $S$-curve contains three regions, namely, (I) $R \le R_{\rm cov}$, (II) $R_{\rm cov} \le R \le R_{rad}$, and (III) $R \ge R_{rad}$ (the corresponding $R_{cov}$ and $R_{rad}$ values for the studied molecules are given in Table 1). $R_{cov}$ marks the extreme distance that corresponds to the completion of the covalent bonding of the molecule electrons according to the multiplicity of its ground state and indicates the onset of restricted/unrestricted Hartree-Fock solutions instability. $R_{rad}$ matches a start of a complete homolytic bond cleavage followed by the formation of two free radicals (see the corresponding arrows indicating the quantities for the $O_2$ molecule in Fig. 1). The intermediate region II with a continuously growing $N_D$ value demonstrates convincingly the growth of electron extraction from the covalent bonding as the corresponding interatomic bond is being gradually stretched. It should be noted that region II is rather narrow and occupies the interval of 1-1.5Å in width.

The analysis of the $N_D(R)$ curves for hydrogen and nitrogen molecules shows that the obtained results are quite realistic. The ground state of both molecules is singlet, and both curves were calculated for this state. As expected, there are no effectively unpaired electros in region I. Consequently, UBS HF and restricted HF solutions coincide and correspond to pure spin states. The number of effectively unpaired electrons in region III is to be 2 and 6 for hydrogen and nitrogen, respectively. As seen in Fig. 1, the $N_D(R)$ curves do approach the asymptotes corresponding to 2 and 6 electrons in this region. Nonzero $N_D$ values obtained in our calculations of the singlet state indicate the obvious singlet instability of the UBS HF

**Table 1.** Critical distances in Å of the onset of the UBS solution instability, $R_{cov}$, and of radical formation, $R_{rad}$, for simple molecules

| *Molecules* | $R_{cov}$ , UBS HF [30] | $R_{cov}$ , UBS DFT (B3-LYP) [29] | $R_{rad}$ |
|---|---|---|---|
| $H_2$ | 1.15 | 1.40 | 2.0 |
| $N_2$ | 1.20 | 1.33 | 2.5 |
| $O_2$ | 1.24 | – | 1.7 |
| $C_2H_4$ | 1.395 | 1.65 | 3.0 |

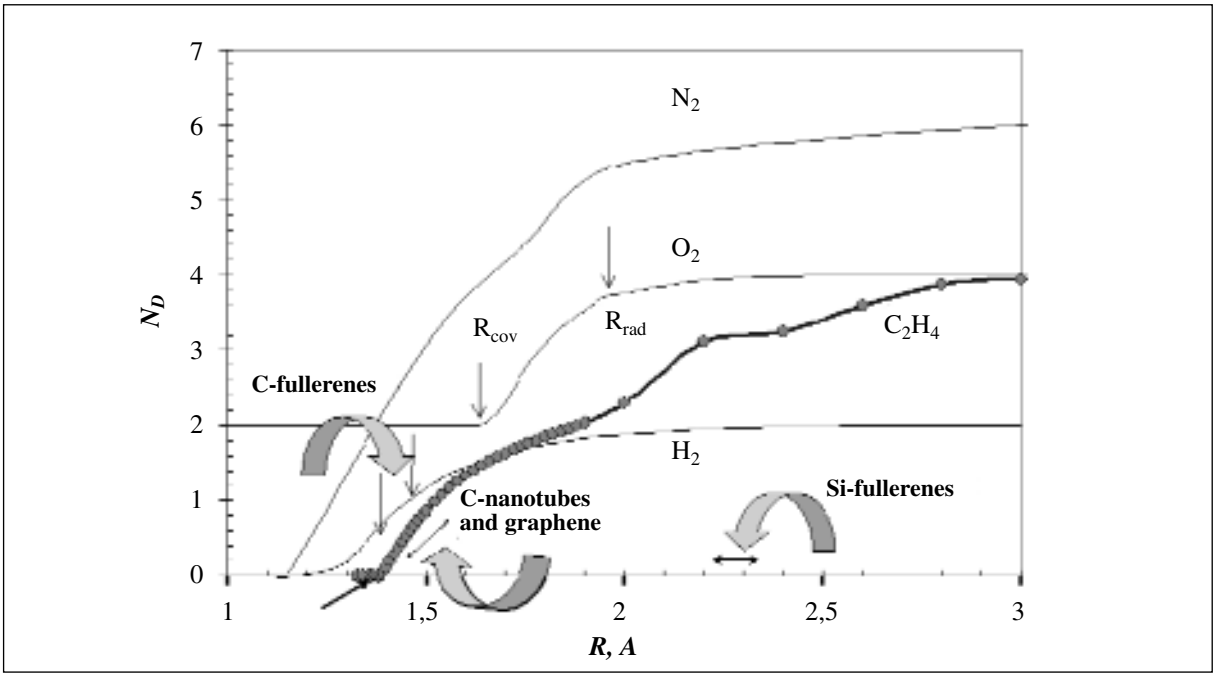


Figure 1. Molecular chemical susceptibility $N_D$ of diatomic molecules and ethylene as a function of the distance between nuclei [11].

solution in this region. The calculations, nevertheless, reproduce correctly the physically expected numbers of unpaired electrons. With oxygen, the analysis of the results obtained in regions I and III shows a similar behavior, but for a triplet state.

In view of carboneous species, $C_2$ pairs are the most interesting. But, the pairs may differ in the number of odd electrons that constitutes 6 for the $C_2$ dimer ($6n$), 4 for acethylene $C_2H_2$ ($4n$), 2 for ethylene $C_2H_4$ ($2n$), and 0 for ethane $C_2H_6$ ($0n$). Naturally, the ethylene molecule is the most appropriate model for aromatic compounds, fullerenes, graphite, graphene, and single-walled carbon nanotubes that are composed of $2n$-bonds. The evolution of the total number of unpaired electrons along the potential curve for the molecule is shown in Fig. 1 by the dotted curve. After calculating the equilibrium structure with the C-C bond of 1.326Å in length, the C-C distance was gradually stretched but kept fixed at a preset value at every next step of calculations while the hydrogen atom positions were optimized. As seen from the figure, the $N_D(R)$ behavior for the molecule is similar to that in the diatomic molecules discussed above. Region I corresponds to covalently bound electrons with $N_D$=0 until $R$ reaches $R_{cov}$ = 1.395Å. On the other hand, when $R$ reaches $R_{rad}$ = 3.0Å, $N_D$ is approaching 4, showing a cleavage of the C-C bond and a total radicalization of the $CH_2$-$CH_2$ pair. The interval between 1.395Å and 3.0Å corresponds to the intermediate case when the odd electrons change their behavior from being totally bonded to totally free.

As shown above, the onset of effectively unpaired electrons follows strictly from a direct dependence of electron pairing on the corresponding interatomic C-C distance in the molecules. This leads to a new numerical factor of the electronic structure and highlights three regions limited by $R_{cov}$ and $R_{rad}$ values that determine extremes (the highest in the first case and the lowest in the second) at which either the covalent bonding is completed or free radical formation starts. The intermediate range between $R_{rad}$ and $R_{cov}$ may be attributed to species with an intermediate-radical character. Therefore, the state of any electron pair in odd-electron carboneous molecules is to depend on the length of the corresponding C-C bond, so that the greater the number of long C-C bonds in the molecule, the greater the total expected number of effectively unpaired electrons. This point was checked for 2*n*- aromatic molecules. As seen from Table 2, the molecules have practically the same set of the C-C bonds while differing in the related bond number, particularly that of long bonds. The $N_D$ values presented in the table show that larger numbers of long bonds in the molecules are accompanied by greater $N_D$ values. The finding made it possible to suggest that the presence of long bonds in fullerenes [5, 20] as well as extending the C-C bond lengths over $R_{cov}$ in carbon nanotubes [29] and graphene [12, 30] causes odd electron unpairing in the species. Two arrows attached to the curve corresponding to ethylene in Fig.1 mark the bond length interval characteristic for fullerenes. A double-headed arrow to the right of the curve matches the bond length interval for SWNTs and graphene. In both cases the intervals are located in the intermediate region above $R_{cov}$. A red point at ~1.4Å corresponds to benzene molecule and indicates an expected absence of effectively unpaired electrons for the molecule which is supported by the data from Table 2. A double headed arrow in the region around 2.3Å corresponds to the interval of Si-Si valent bonds lengths. The interval is located in the region where the radicalization is either very considerable or fully completed. This means that the $sp^2$ configuration of odd electrons in siliceous species is highly unfavorable (see a detailed discussion of the problem in Section 6).

In the performed UBS HF calculations $R_{cov}$ = 1.395Å is an extreme above which electron unpairing related to any 2*n* C-C bond may occur. Bond lengths of fullerenes and carbon nanotubes exceed the distance by ~0.1Å. The small value makes the accuracy of the $R_{cov}$ determination rather crucial which puts a question addressed the used computational technique. As for the ethylene molecule, a comparative study of the homolytic cleavage of the C-C bond by different techniques has shown [31], that critical distances $R_{cov}$ form a series

$$R_{cov}: \text{UHF}<\text{B3-LYP}<\text{B-P}<\text{S-VWN}, \quad (12)$$

where B3-LYP, B-P, and S-VWN correspond to different DFT functionals used in the calculations with a split valence plus polarization basis set. As seen from Table 1, the difference between UBS HF and UBS DFT values exceeds 0.1Å, so that no electron unpairing should be expected for fullerenes, SWNTs, and graphene according to the DFT data. However, series (12) just visualizes a functional-pressed character of the UBS DFT solution that makes the approach less sensitive to the effectively unpaired electrons behavior while UBS HF approach suggests results that are consistent with the available many-body CI calculations. We shall come back to the discussion of the topic in Sections 4.2, 4.5, and 4.6.

## 4. Odd-electron-enhanced chemical reactivity

### 4.1. Chemical reactivity of carbon nanotubes

The increasing number of physical, chemical, and biomedical applications of carbon nanotubes requires chemical modification of the latter to make them more amenable to rational and predictable manipulation [32]. Two main strategies concerning non-covalent [33] and covalent [34] functionalizations have been elaborated and have gained large practical success and achievements (see comprehensive reviews [35-42]). However, controllable

**Table 2.** Effectively unpaired electrons in aromatic molecules, UBS HF singlet state [30]

| *Molecules* | *C-C bond length, Å* | | | | $N_D$ |
|---|---|---|---|---|---|
| | *Number of bonds* | | | | |
| Benzene | 1.395 | | | | 0.05 |
| | 6 | | | | |
| Naththalene | 1.385 | 1.411 | 1.420 | 1.430 | 1.483 |
| | 4 | 2 | 4 | 1 | |
| Anthracene | 1.387 | 1.410 | 1.421 | 1.435 | 3.003 |
| | 4 | 6 | 4 | 2 | |
| Tetracene | 1.388 | 1.410 | 1.421 | 1.436 | 4.320 |
| | 4 | 8 | 6 | 3 | |
| Pentacene | 1.388 | 1.411 | 1.420 | 1.436 | 5.540 |
| | 4 | 10 | 8 | 4 | |

functionalizing techniques, which can provide carbon nanotubes tailoring in a determinable manner, are far from being completed; more investigations are required to elucidate the nature and locality of covalently attached moieties. Due to extreme complication of native carbon nanotubes as well as difficulties in their separation and individual studying, a considerable load connected with looking for answers is put on the shoulders of computational approaches. Starting in [36], a number of calculations have been performed [43-53].

Not very long ago the main concept of the connection between the electronic structure and chemical reactivity of CARBON NANOTUBEs was based on the Haddon approach [54] that attributed the reactivity of fullerenes to the strain engendered by their spherical geometry as reflected in pyramidalization angles of carbon atoms. Just as in the case of fullerenes, curvature-induced pyramidalization and misalignment of the π-orbitals of the carbon atoms [55-57] induces a local strain in a defect-free carbon nanotube. This concept made allowance for explaining the difference between the reactivity of a SWCARBON NANOTUBE end cap and sidewall in favor of the former, and gave a simple explanation of the reactivity increase while the SWCARBON NANOTUBE diameter decreases. Further development of the approach turned out to be useful for considering the reactivity of the convex and concave sidewalls of SWCARBON NANOTUBEs towards addition reactions [43, 44].

The Haddon approach was quite productive but basically empirical while more sophisticated theoretical approaches were needed. Various DFT techniques actively explored during the last years with respect to the chemical functionalization of carbon nanotubes, to name a few [46- 53], were a natural response to the requirement. However, a lot of severe limitations were usually implied when using the technique. This concerns 1) the aromaticity concept attributed to the electronic structure of the tubes which results in the closed-shell approximation for wave functions (that concerns the restricted DFT approach); 2) the periodic boundary conditions along the tubes which restrict the tube area consideration to sidewall only leaving the tube ends, the most active spots on the tube, as was shown [29], outside the consideration; 3) the absence of atomically matched characteristics that could exhibit the chemical reactivity of the tube atoms; 4) a *post factum* character of simulations that were aimed at obtaining the energy and structural data consistent with experimental findings by adapting the functional used. The most crucial is the first assumption in view of weakly interacting odd electrons in carbon nanotubes. When the problem is considered in the framework of the aromaticity concept, this means strong coupling between the electrons so that odd electrons are covalently coupled in pairs similarly to π electrons of benzene molecule. The only UBS DFT calculation has been known so far [57] that thoroughly analyzed the singlet state of cyclacenes and short zigzag SWCARBON NANOTUBEs. It was shown that

the energy of the UBS DFT singlet state was lower than that of the restricted DFT singlet that pointed to the open-shell character of the singlet state. The finding is of great importance exhibiting the falsity of aromaticity-based concept for quantitative description of the electronic states of carbon nanotubes on the DFT platform.

Firstly applied to two fragments of (4,4) defect-free and (4,4) (5-7) defect SWCARBON NANOTUBE as example [29], UBS HF approach has demonstrated that $N_{DA}$ values appeared and followed in synchronism with the excess of C-C distance that separates two odd electrons over the limit value $R_{cov} \cong 1.395$Å. Therefore, the $N_{DA}$ map which describes the tube atoms atomic chemical susceptibility is tightly connected with the tube structure thus highlighting the distribution of the C-C bond length excess over the tube. To prove the statement, an extended set of fragments of (n,n) and (m,0) SWCARBON NANOTUBEs has been considered later on [11]. Calculations were performed in semiempirical approximation by using AM1 version of the CLUSTER-Z1 program [58] that provides stable UBS HF calculations in singlet states supplemented by the calculations of $N_D$ and $N_{DA}$ quantities. Particular attention was given to the initial guess to both $P^{\alpha}$ and $P^{\beta}$ matrices when performing calculations in the singlet state. An obvious choice in setting these matrices to zero and using $H^{core}$ as the initial guess to both matrices is followed by producing identical orbitals for α and β spins [28]. To avoid the complication, the relevant matrices were obtained in due course of one-point-geometry calculations in the triplet state (or any other high spin state) and then were input as the initial guess for the singlet calculations.

#### 4.1.1. (4,4) single-walled carbon nanotubes

Equilibrium structures of the studied fragments were obtained in due course of the structure optimization when seeking the energy minimum and are presented in Fig. 2 and Fig.3. Numbered from NT1 to NT9 the fragments form three groups. The first group (Fig. 2) involves three fragments related to short defect-free (4,4) SWCARBON NANOTUBEs different by the end structure. One end of all fragments is capped while the other is either open but hydrogen terminated (NT1) and empty (NT2), or capped (NT3). The attached hydrogens are not only service terminators but present real hydrogenation of the tube open end. The collection is added by a defect (4,4) SWCARBON NANOTUBE (NT4) with a Stone-Wales pentagon-heptagon pair. The second group (Fig.3) involves fragments NT5 and NT6 that present capped-end & open-end (4,4) SWCARBON NANOTUBEs but different by the termination of the open end. They both differ from fragments NT1 and NT3 by four atom rows elongation. The third group (Fig. 3) combines NT7, NT8, and NT9 fragments of (4,4) SWCARBON NANOTUBEs with both open ends but different by hydrogen termination. The fragment sidewall is longer by one atom row in comparison with that of the second group. To sum up, the fragments allow considering the following structure effects on the $N_{DA}$ distribution caused by i) endcaping; ii) terminating or emptying open ends; iii) introducing a pair of pentagon-heptagon defects; iv) the tube sidewall elongation.

##### *Fragments of group 1*

Eight hydrogen atoms terminate the NT1 open end. The tube atoms are numbered from the cap towards the open end following their symmetrical disposition with respect to both $C_2$ axis and the symmetry plane passing through the axis normally to the paper sheet. The numbering of atom rows proceeds in the opposite direction. This enumeration will be retained in what follows when presenting calculation data for other fragments.

As shown in [29], the dominating majority of C-C bonds of the tube is longer than the limit $R_{cov}$ =1.395Å, so that the large total number of effectively unpaired electrons for the tube $N_D$= 32.38 does not look strange. The distribution of these electrons over the atoms forms the ACS $N_{DA}$ map that is shown in Fig. 4(a). As seen from the figure, the map shape supports $C_{2v}$

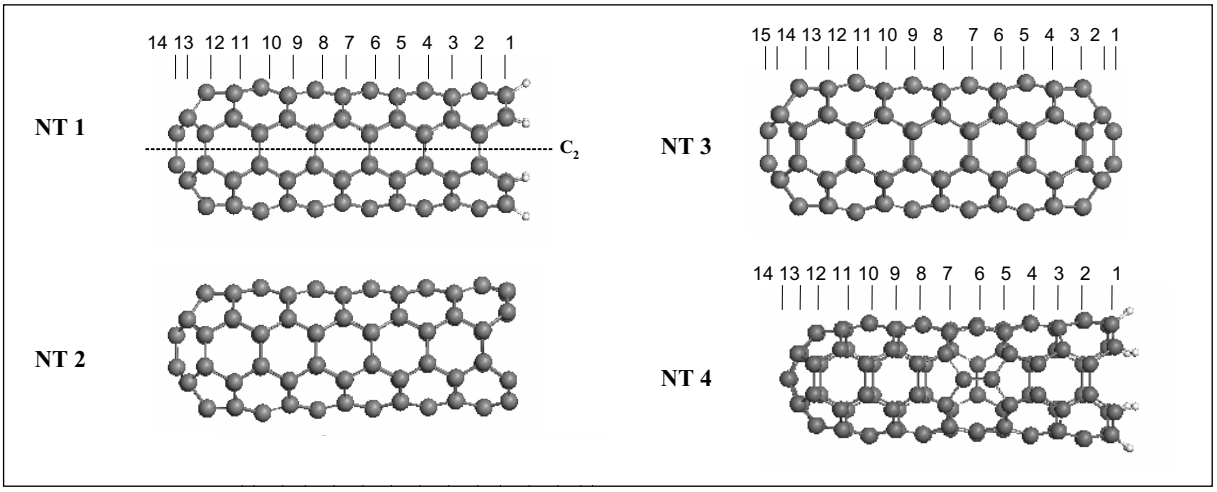


Figure 2. Equilibrium structures of (4,4) single-walled carbon nanotube fragments. Group 1 (NT1, NT2, NT3, and NT4). UBS HF singlet state [11].

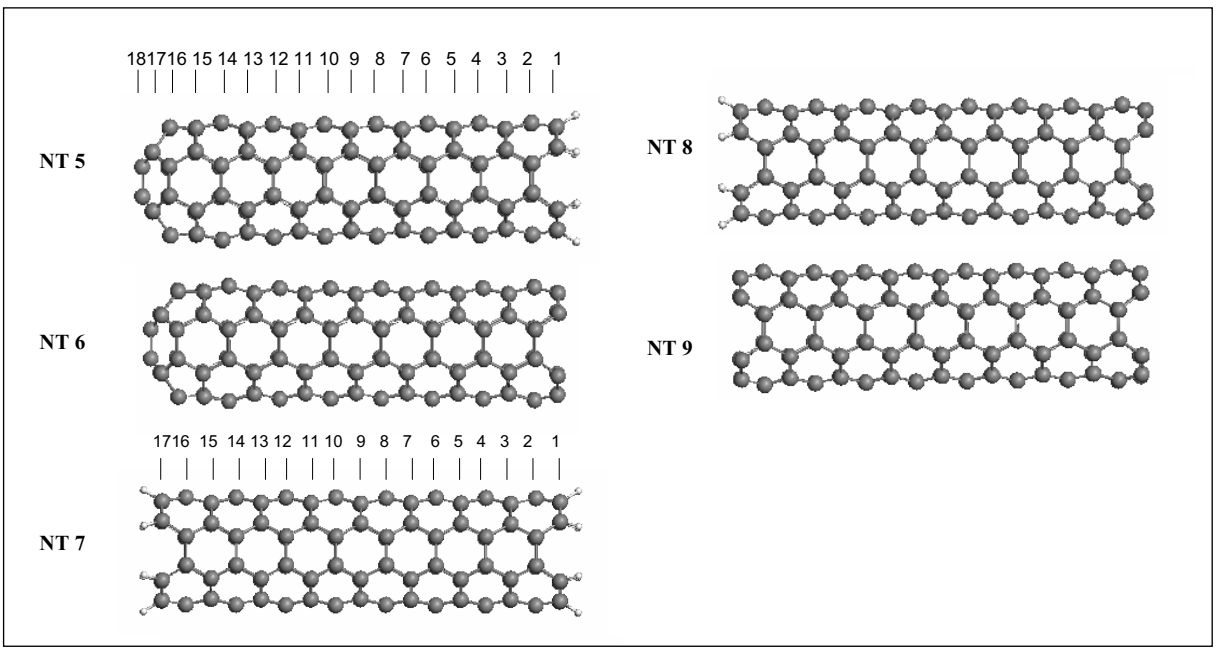


Figure 3. Equilibrium structure of (4,4) single-walled carbon nanotube fragments of group 2 (NT5 and NT6) and group 3 (NT7, NT8, and NT9). UBS HF singlet state [11].

symmetry of the atom arrangement. According to the map, the tube can be divided into three regions. The first is related to the cap with adjacent atoms and covers rows 9-14. The second concerns mainly the tube sidewall and covers rows 4-8. The third refers to the open end terminated by hydrogen atoms and covers rows 1-3. The biggest non-uniformity of the $N_{DA}$ distribution is characteristic of the cap region. One should pay attention to the fact that the largest $N_{DA}$ values belong to atoms which are characterized by the largest C-C bond length and vice versa. As for the sidewall region, the $N_{DA}$ distribution is practically uniform with the $N_{DA}$ value scatter not bigger than 0.5% that is consistent with quite uniform distribution of C-C bond lengths as well. The $N_{DA}$ distribution in the end region is significantly affected by the hydrogenation. But in this region there is a direct correlation between $N_{DA}$ values and lengths of C-C bonds as well. Therefore, the C-C bond length is actually a controlling factor in the distribution of the density of the effectively unpaired electrons over atoms.

The curve with dots in Fig. 4(a) presents the free valency of the tube atoms calculated in accordance with the relation

$$V_A^{free} = N_{val}^A - \sum_{B \neq A} K_{AB} \tag{13}$$

where $N_{val}^A$ is the number of valence electrons of atom $A$ and $\sum_{B \neq A} K_{AB}$ is the generalized bond index

$$K_{AB} = \left|P_{AB}\right|^2 + \left|Sp_{AB}\right|^2 . \tag{14}$$

Here, the first term is the Wiberg bond index [59] and the second one is determined by the spin density matrix (see [60] for details). The excellent agreement of the two values shows that the $N_{DA}$ map does exhibit a quantitative measure of free valency and/or atomic chemical susceptibility. From this viewpoint, the tube cap is the most reactive part, while the tube sidewall is more passive with ill-pronounced selectivity along the tube.

Removing hydrogen atoms at the tube open end, one obtains the $N_{DA}$ map of NT2 fragment shown in Fig. 4(b). A tremendous contribution of the end atoms obviously dominates on the map. It is due to the fact that the ethylene-like (*2n*) C-C bonds (see Section 3) are replaced by the acetylene-like (*3n*) bonds at the tube end where each atom has not 1 but 2 odd electrons. The transformation naturally results in increasing the total number of effectively unpaired electrons $N_D$ from 32.38 up to 39.59. The injection of additional effectively unpaired electrons disturbs the $N_{DA}$ map of the hydrogen-terminated tube shown in the figure by bars quite considerably. It is important to note that the changes occur not only in the vicinity of the open end within rows *2* and *3* that is quite reasonable, but influence the opposite cap end (rows *14-11*). Practically no changes occur along the tube sidewall which seems to serve as a peculiar resonator for the electron conjugation. Addressing the chemical activity of the tube, dominant activity of the empty end atoms is evident

When the other end is capped, fragment NT3 ($N_D$=33.35) becomes highly symmetrical ($D_{2h}$) that is reflected in its $N_{DA}$ map shown in Fig. 4(c). The $N_{DA}$ distribution of the fragment is specularly symmetrical with respect to the atoms of row *8* in the middle. As seen from the figure, besides the second cap region, the addition of the second cap results in no changes in the distribution which is characteristic of the one-cap fragment NT1.

The defect introduction in the NT4 fragment was purposely made above the symmetry axis to distinctly violate symmetry of the perfect tube from $C_{2v}$ to $C_s$ so one could expect a noticeable alteration of the $N_{DA}$ map of the perfect tube caused by lowering the symmetry. A comparative analysis of the maps of the perfect and deformed tubes presented in Fig. 5 shows that the main alterations concern the atoms of rows 5-7 that are involved in the defect structure. The remainder part of the sidewall region as well as the cap and open end regions of the tube are much less affected. And nevertheless, while small, the changes caused by the defect touch upon all atoms of the 12-row tube.

The significance of the open end termination can be traced through charge characteristics of the fragments as well. In series NT1, NT2, NT3 dipole moments of the fragments are 9.93, 0.44, and 0.03 D, respectively. A drastic drop of the value when terminating hydrogen atoms are removed is evidently connected with the charge redistribution over the tube atoms. Fig. 6 presents the corresponding plotting for the fragments. Bars in the figure show the charge distribution along NT1 fragment. The atom enumeration coincides with that of the $N_{DA}$ map in Fig. 4(a). As seen from the figure, attached hydrogens as well as adjacent carbon atoms provide the main contribution to the distribution. The influence of terminators is still sensed at other two atomic layers towards the tube cap. The remainder tube sidewall is practically uncharged, and a weak charging of atoms appears again only at the end cap. The acquired total negative charge is fully compensated by the positively charged hydrogen atoms.

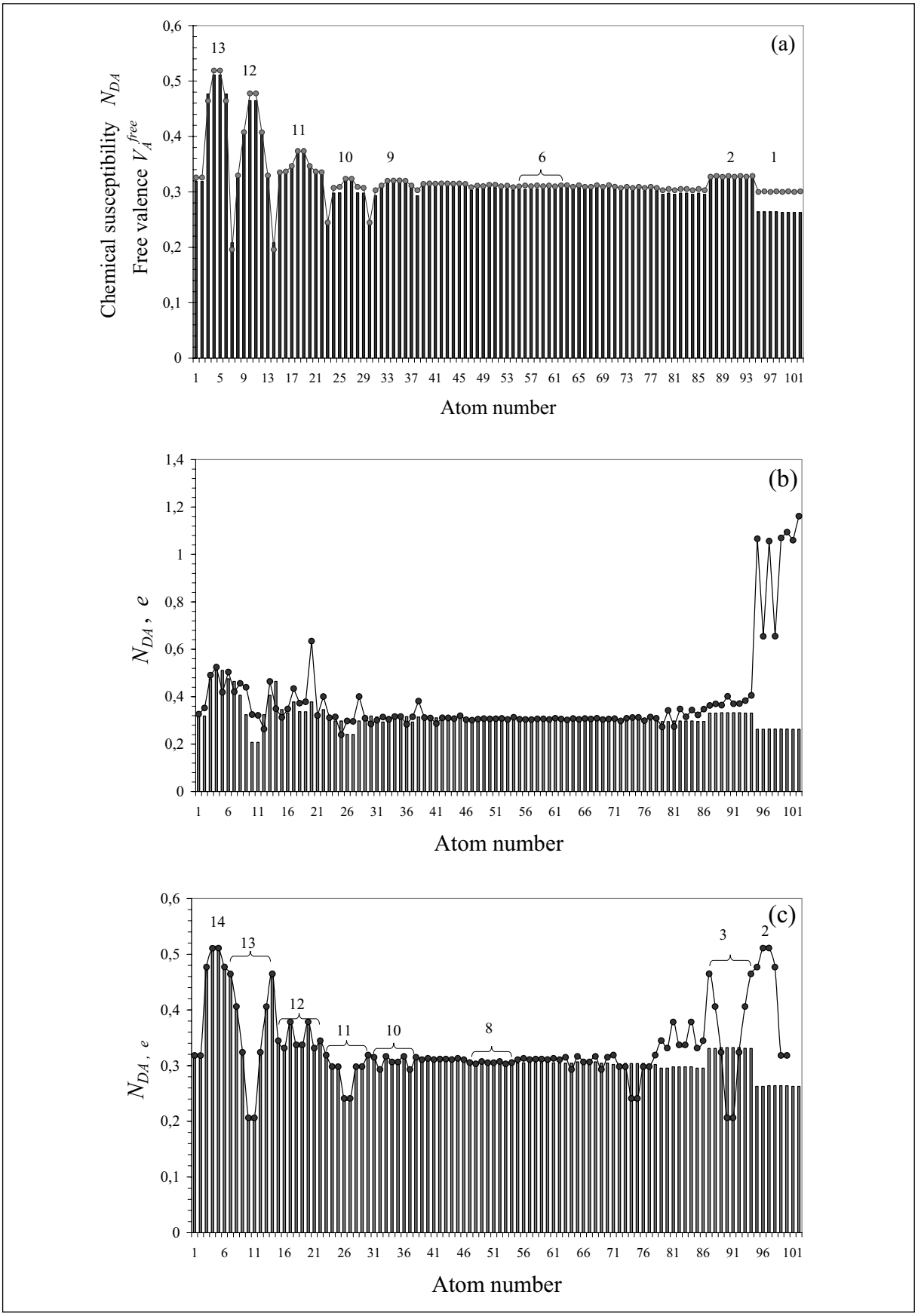


Figure 4. Atomic chemical susceptibility $N_{DA}$ maps. a. NT1 fragment; histogram exhibits $N_{DA}$ distribution, curve with dots presents free valence. b. NT1 (bars) and NT2 (curve with dots) fragments; c. NT1 (bars) and NT3 (curve with dots) fragments. Numerals match atom rows [11].

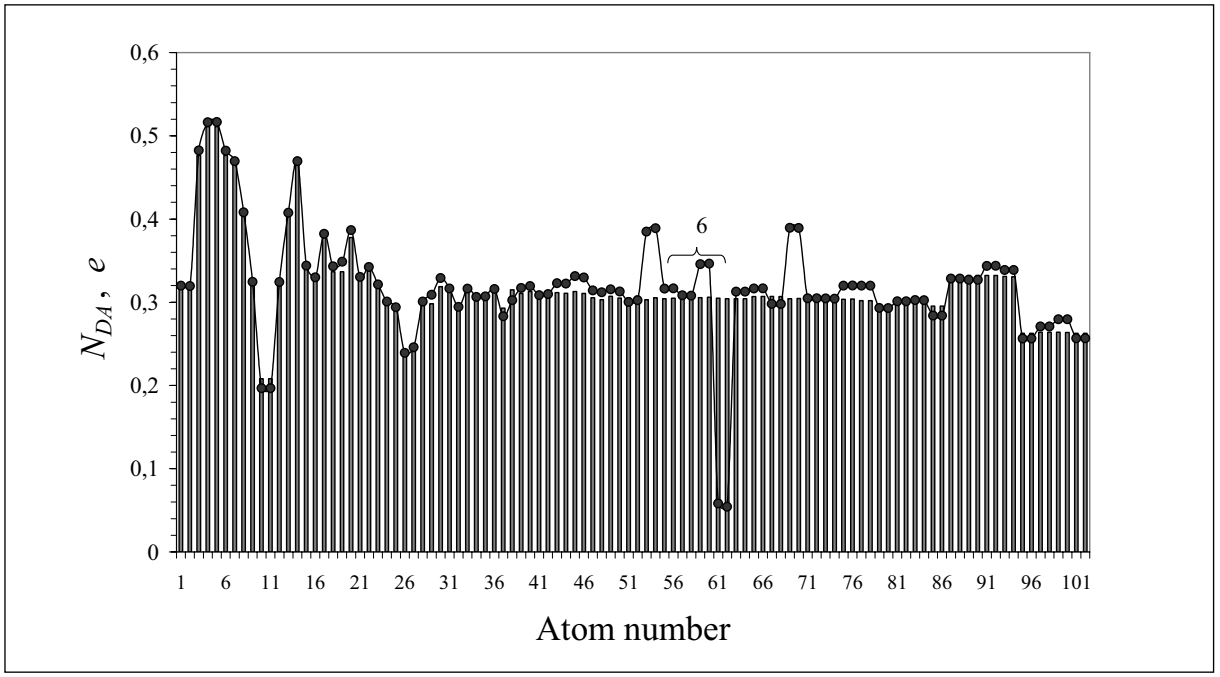


Figure 5. Atomic chemical susceptibility $N_{DA}$ maps of NT1 (bars) and NT4 (curve with dots) fragments [11].

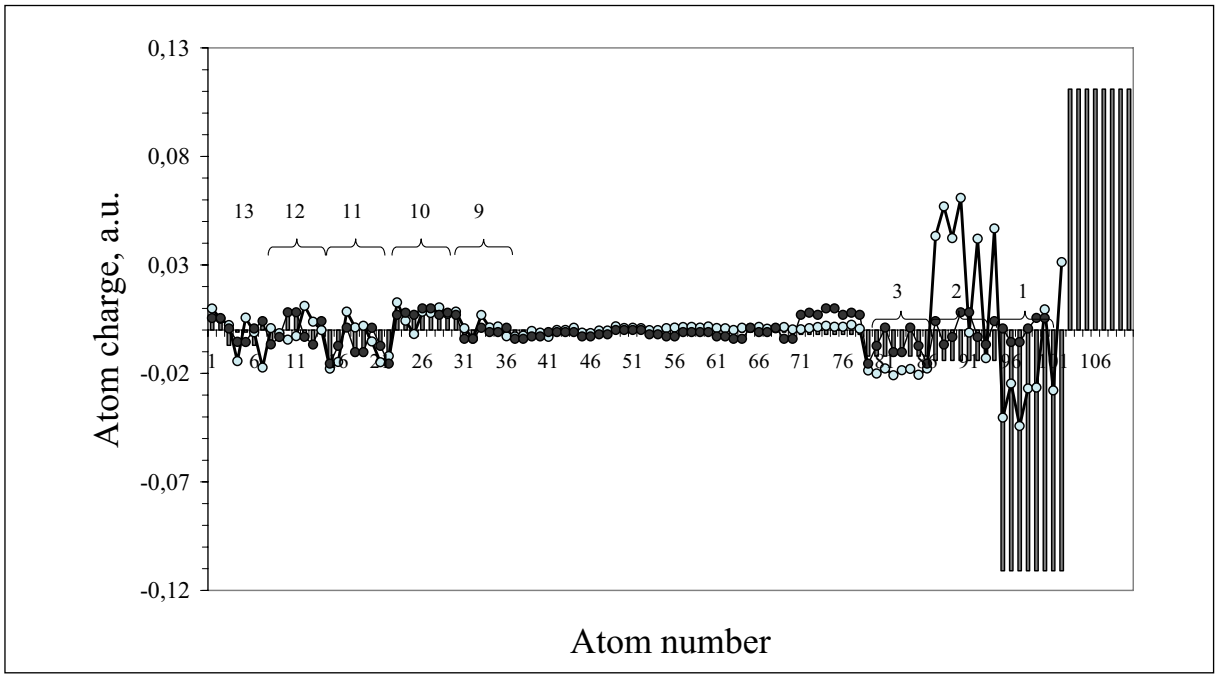


Figure 6. Charge distribution over atoms of fragments of group 1. Bars, curve with light and dark dots plot data for NT1, NT2, and NT3, respectively. Numerals match atom rows of fragments NT1 and NT2 [11].

However, the significantly charged "tail" of the fragment provides a high value of the dipole moment.

When hydrogen atoms are removed the charge map is reconstructed. First, it concerns end carbon atoms whose charge greatly decreases but the charging area is still large covering rows *1-3*. Besides, the charge redistribution is seen in the cap region as well while along the tube sidewall changes are small. And again, as in the case of the $N_{DA}$ distribution, one can speak about a resonant character of the disturbance transfer along the tube sidewall. One might suggest that this very charge transfer along the tube results in so significant decrease of the dipole moment value in spite of a still considerable charge on the tube open end.

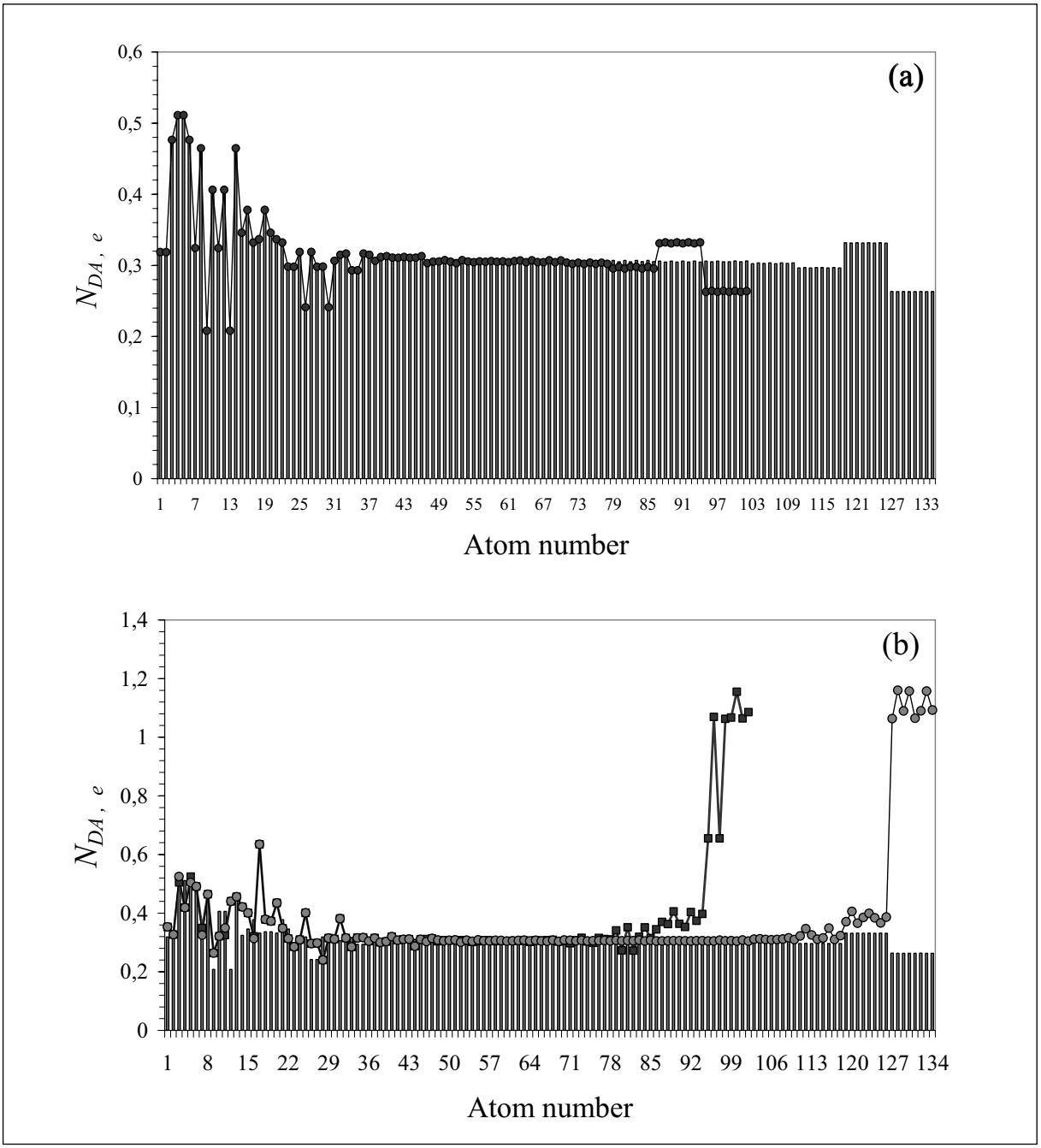


Figure 7. Atomic chemical susceptibility $N_{DA}$ maps. a. NT5 (bars) and NT1 (curve with dots) fragments; b. bars, curves with light and dark dots plot data for NT5, NT6, and NT2 fragments, respectively [11].

Replacing the open end by the second cap does not violate the charge distribution in the region of the first cap and simply duplicates it in the region of the second cap just making the total tube $N_{DA}$ map specularly symmetrical with respect to the middle row of atoms. Highly symmetric and having low value, the charge distribution produces an exclusively small dipole moment.

***Fragments of group 2***

The $N_{DA}$ maps given for fragments NT5 and NT6 in Fig. 7 show the following. Like for the members of group 1 considered in the previous Subsection, the $N_{DA}$ map of the fragments consists of three regions related to the cap end on the left, open end on the right, and an extended tube sidewall. As for both end regions, the data for the elongated tube fully

reproduce those for the shorter one, irrespectively of the open end being either hydrogen terminated (Fig. 7(a)) or empty (Fig. 7(b)). Similar behavior of the map should be expected if the open end is capped. The only difference in the distributions related to shorter and longer fragments consists in expending the distributions fraction related to the tube sidewalls. Therefore, the $N_{DA}$ map may be presented as consisting of three fragments MapI, MapII, and MapIII. In the case of two cap ends, MapIII should be replaced by MapI. As seen from Fig. 7, MapI covers region of first (and/or last) 37-40 atoms. MapIII is spread over 24 last atoms. MapII takes the remainder space which depends on the tube length.

***Fragments of group 3***

Group 3 covers fragments with both open ends. Similarity in the tube length of fragments from group 2 and group 3 allows revealing the changes caused by replacing one or two capped ends by open ends.

Fig. 8(a) presents a comparative view of $N_{DA}$ maps of fragments NT5 and NT7 that have similar right open ends terminated by hydrogen and different left ends presented by the cap in the case of NT5 and by the hydrogen terminated open end in NT7. The comparison shows that if three-region pattern described above is characteristic of capped NT5 fragment, this can not be said about NT7. The $N_{DA}$ map in this case is specularly symmetrical with respect to the middle row but is quite inhomogeneous with a peculiar step-like character reaching minimum at the tube center. It should be noted nevertheless that the step character related to the last three rows on the right end is the same as for the NT5 open end.

Removing hydrogen atoms on the right end of NT7 brings back the $N_{DA}$ map of fragment NT8 to the three-region form described in the previous Subsection (see Fig 8(b)) but expressed as MapIII+MapII+MapIII$^{*}$. MapII and MapIII have the same shape as previously while MapIII$^{*}$ concerns 24 last atoms after removing hydrogen terminators. When the remaining eight terminators are removed on the left end, the $N_{DA}$ map of fragment NT9 acquires a new three-region form expressed as MapIII$^{**}$+MapII+MapIII$^{*}$. As a whole, the map becomes almost specularly symmetrical with respect to the middle row of atoms while MapIII$^{**}$ somewhat differs from MapIII$^{*}$. When fragment NT9 is formed from NT7 avoiding the NT8 stage, MapIII$^{**}$ is fully identical to MapIII$^{*}$.

### 4.1.2. (n,n) and (m,0) single-walled carbon nanotubes

***(n,n) SWCARBON NANOTUBEs***

The obtained results show that the three-region pattern of the $N_{DA}$ maps is generally supported for all studied (n,n) fragments. Thus, the graphical views of the $N_{DA}$ maps for (5,5); (6,6); (7,7); and (8,8) members are quite similar to those of the (4,4) set whilst being naturally different numerically. The corresponding $N_{DA}$ values are summarized in Table 3. When the scattering of data is big, the related interval of the value is shown. The analysis of the data given in the table makes allowance for exhibiting the dependence of the ACS on the SWCARBON NANOTUBE diameter. As seen from the table, the dependence is different in different regions. Thus, ACS of the H-terminated ends does not show any dependence at all. Carbon atoms of the empty ends form two groups which are characterized by different $N_{DA}$ values. The bigger value of 1.16 does not change when the diameters increases while the lower one drops from 1.06 to 0.67 when passing from (4,4) SWCARBON NANOTUBE to (5,5) one and then remains unchanged. The side wall ACS decreases gradually when the diameter increases and approaches a constant value when the diameter grows further. Qualitatively, the ACS behavior in this region looks like that expected on the basis of the Haddon approach. Obviously, the $N_{DA}$ values will approach the ones of a graphene sheet when the diameter further increases. As for the cap region, large scattering of the ACS values as well as their peculiar change reflect a severe reconstruction of the C-C bond net in the region

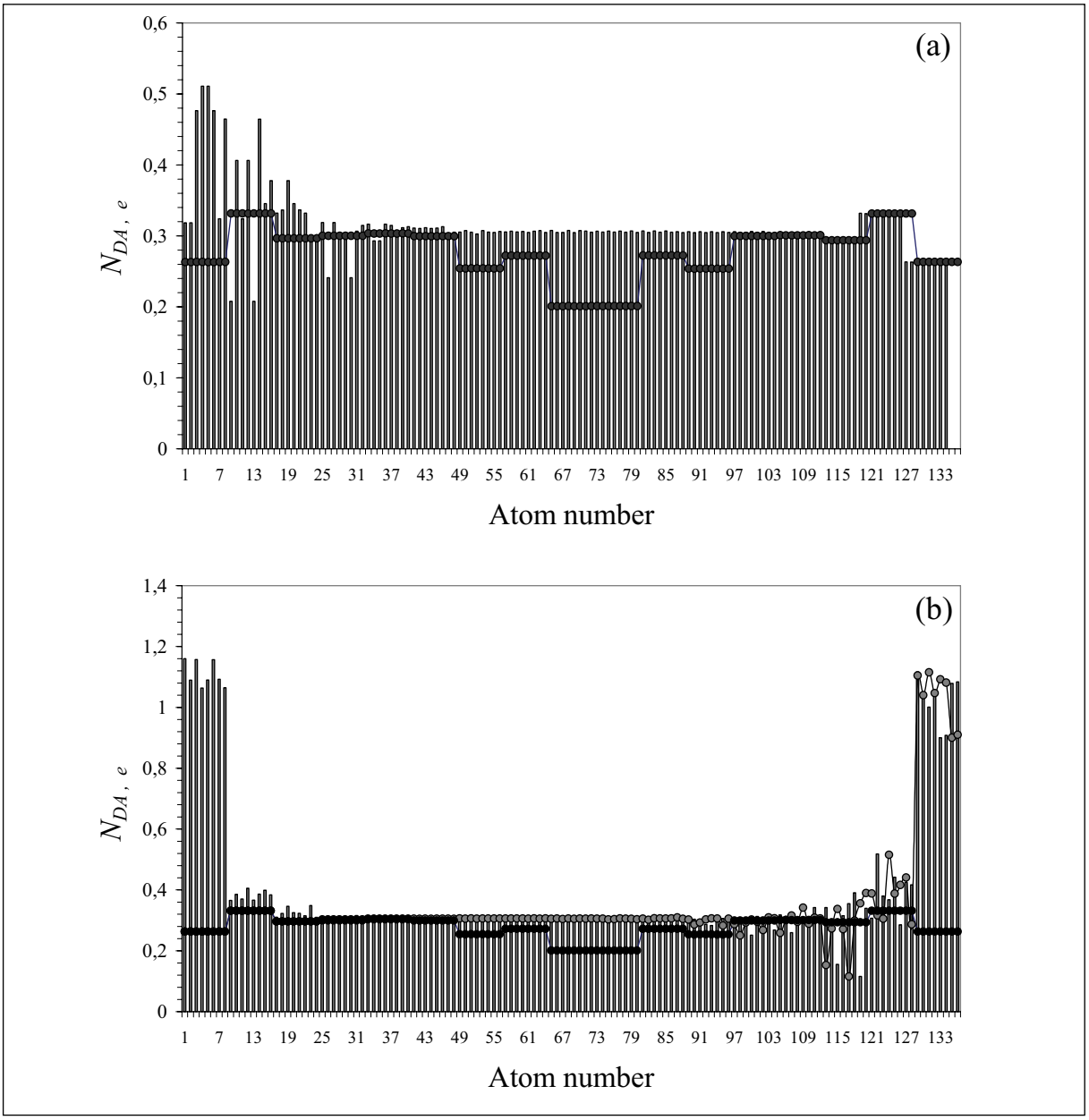


Figure 8. Atomic chemical susceptibility $N_{DA}$ maps. a. NT5 (bars) and NT7 (curve with dots) fragments; b. bars, curves with light and dark dots plot data for NT9, NT8, and NT7 fragments, respectively [11].

adapting it to a minimal stress of the tube body as a whole and its cap end, in particular. From this viewpoint, small $N_{DA}$ values at the cap of the (5,5) tube are obvious. The tube symmetry is $C_{5v}$ and the cap structure is comfortably centered around pentagon. The C-C bonds are the least stressed and lengthened that causes the smallest $N_{DA}$ values.

As seen from Table 3, oppositely to the previous case, scattering of the $N_{DA}$ values of tubes (9,9) and (10,10) is significant. Particularly, small $N_{DA}$ values in the sidewall and open H-terminated regions should be mentioned. This feature was attributed to the great stress of the tube bodies that is clearly seen in Fig.9. As follows, in this case one cannot expect regular C-C bond lengths distribution not only in the cap region, but on sidewall and end atoms as well. The observed decrease of the $N_{DA}$ values is connected with the C-C bond shortening that reflects the body stress. At the same time, the largest values in the sidewall and H-terminated end region are similar to those of the previous group and clearly show their saturation under the tube diameter growing. Similar characteristics might be expected for the tube of larger diameter as well.

**Table 3**. Atomic chemical susceptibility of single-walled carbon nanotubes [11]

| | Diameter, Å | $N_{DA}$[1], *e* | | | |
|---|---|---|---|---|---|
| | | Cap | Sidewall | Open ends | |
| | | | | Empty | H-terminated |
| **SWCNTs (n,n)**[2] | | | | | |
| **4,4** NT5, NT5* | 5.76 | 0.51-0.32 | 0.31 | 1.16; 1.06 | 0.26 |
| **5,5** NT10, NT10* | 7.06 | 0.17-0.03 | 0.30-0.26 | 1.16; 0.66 | 0.26 |
| **6,6** NT11, NT11* | 8.34 | 0.29-0.06 | 0.25 | 1.16; 0.67 | 0.26 |
| **7,7** NT12, NT12* | 9.79 | 0.34- 0.06 | 0.26 | 1.07; 0.67 | 0.25 |
| **8,8** NT13, NT13* | 10.91 | 0.34-0.06 | 0.24 | 1.16-1.06; 0.67-0.68 | 0.25 |
| **9,9** NT14, NT14* | 12.64 | 0.26-0.04 | 0.23; 0.03 | 1.12-0.67 | 0.25; 0.09 |
| **10,10** NT15, NT15* | 14.00 | 0.26-0.05 | 0.23; 0.19-0.17; 0.10-0.06 | 1.16-0.97; 0.68 | 0.24-0.22; 0.19-0.17; 0.06-0.02 |
| **SWCNTs (m,0)** | | | | | |
| **8,0** NT16, NT16* | 6.20 | 0.45-0.11 | 0,29-0.28 | 1.80-1.11 | 0.49-0.24 |
| **10,0** NT17, NT17* | 7.97 | 0.35- 0.19 | 0.26 | 1.36;1.14 | 0.45 |
| **12,0** NT18, NT18* | 9.61 | 0.37-0.04 | 0.26-0.21 | 1.36;1.15 | 0.47-0.11 |

[1] Within each cell the data are presented by single numbers or a set of single numbers when their scattering around the corresponding number is less than 0.01 *e*. Otherwise, the data are presented by intervals or groups of intervals.
[2] NT*n* nominates capped-end/H-terminated-open-end fragment while NT*n** does the same for the ones after removing hydrogen atoms from the open end (see NT5 and NT5* (that is NT6) in Fig.3). Fragments from NT14 till NT18 are shown in Fig.9.

In spite of large scattering of the $N_{DA}$ data in the sidewall region, their distribution retains a regular view. The matter is that the scattering takes place within each individual row of the sidewall while being repeated regularly over rows. The $N_{DA}$ distribution within one row of the studied tubes is shown in Fig.10. As seen from the figure, it looks quite similar for both tubes as well for other rows of the two ones.

***(m,0) SWCARBON NANOTUBEs***

While (n,n) SWCARBON NANOTUBEs all are semiconductive, the (m,0) SWCARBON NANOTUBEs family consists of both semiconductive and metallic (really, semimetallic) tubes depending on whether *m* is divisible by 3. Therefore, a series of (8,0), (10,0), and (12,0) fragments covers two semiconductive and one metallic tube and offers two new aspects for the comparative study. The latter concerns changes of the $N_{DA}$ maps caused by (1) replacing armchair open ends of (n,n) tubes by zigzag ones for (m,0) family and (2) changing the tube conductivity within the (m,0) family.

In response to the first inquiry, the calculations performed in [11] have revealed a large similarity in the behavior of (n,n) and (m,0) fragments. A comparative view on the $N_{DA}$ maps of (4,4) and (8,0) fragments that both are semiconductive and close by diameter is presented in Figs.11a and 11b. As seen from the figure, $N_{DA}$ maps of the two tubes are both qualitatively and quantitatively similar. First, the maps consist of three parts related to variable $N_{DA}$ values at capped and open ends and to rather homogeneous quantities along the tube sidewalls. In both cases the open empty ends are the most chemically reactive. Following these places in activity are the end caps and sidewall. Second, not only shape of the $N_{DA}$ maps but numerical plottings related to end caps and sidewalls (Table 3) are practically the same. The only

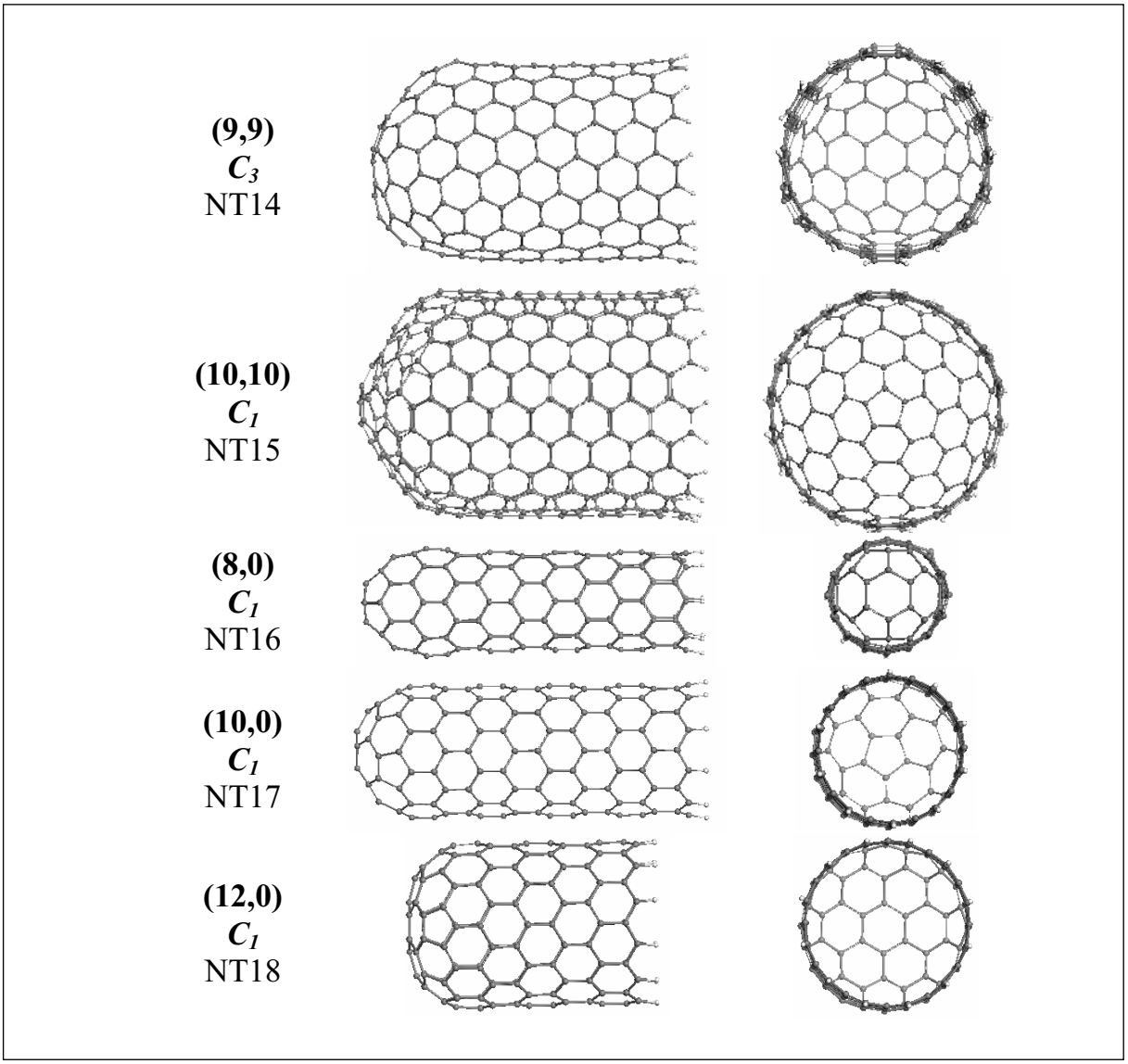


Figure 9. Equilibrium structures of armchair (9,9) (NT14) and (10,10) (NT15) fragments and zigzag (8,0) (NT16), (10,0) (NT17), and (12,0) (NT18) SWCNT fragments in two perpendicular projections [11].

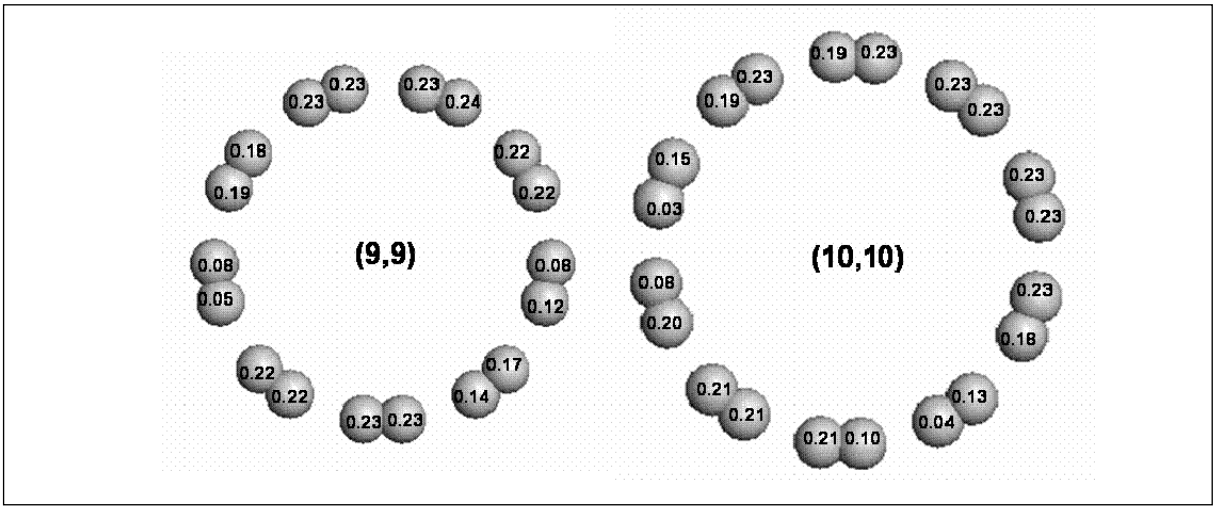


Figure 10. Atomic chemical susceptibility $N_{DA}$ maps of the cross sections of (9,9) (NT14) and (10,10) (NT15) SWCNTs [11].

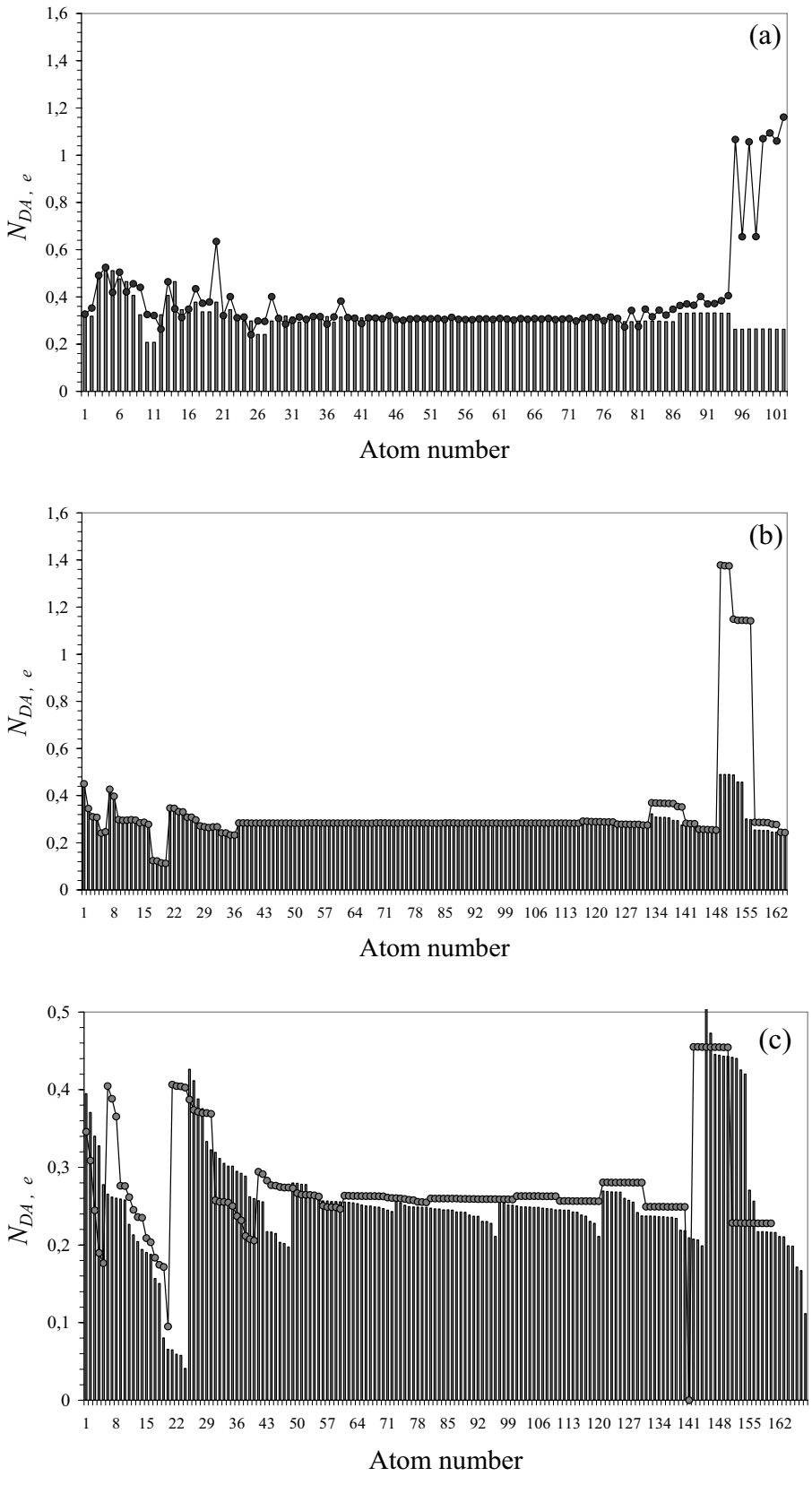


Figure 11. Atomic chemical susceptibility $N_{DA}$ maps. a. (4,4,) SWCNT. Histogram and curve with dots are related to fragments NT5 and NT6, respectively. b. (8,0) single-walled carbon nanotube. Histogram is related to NT16 fragment while curve plots $N_{DA}$ quantities for NT16* when hydrogen atoms are removed from the open end of NT16. c. NT17 (histogram) and NT18 (curve) fragments [11].

difference concerns zigzag open ends, both H-terminated and empty, that exhibit about 15% increase of the reactivity in comparison with the one of armchair ends. These regularities remain to a great extent for SWCARBON NANOTUBEs of bigger diameter: compare the data in Table 3 for (6,6) and (10,0) as well as for (7,7) and (12,0) tubes.

The latter is of particular interest since (7,7) SWCARBON NANOTUBE is semiconductive while (12,0) is metallic. A more detailed comparison between the maps of the tubes of different conductivity is visualized in Fig.11c for (10,0) and (12,0) SWCARBON NANOTUBEs belonging to the same family. As seen from the figure, plottings for both tubes are well similar in both shape and numbers and do not exhibit any remarkable characteristic difference that might be related to changing in the tubes conductivity. Therefore, the chemical reactivity of atoms of both semiconductive and metallic SWCARBON NANOTUBEs is comparable that should not cause different behavior of the tubes with respect to similar chemical reactions. This is consistent with the reality when one faces the problem of using sidewall covalent chemistry for tube separation [61]. Partial lucks in achieving the goals of distinguishing semiconductive and metallic tubes by using chemical modification seem to be connected with the peculiarities of intermolecular interaction between the tube and corresponding additives caused by the donor-acceptor interaction.

### 4.2. General view on single-walled carbon nanotubes chemical reactivity

Exhibited peculiarities of the obtained SWCARBON NANOTUBE ACS ($N_{DA}$) maps allowed making the following conclusions concerning addition reactions to be expected [11].

1. The space of chemical reactivity of any SWCARBON NANOTUBE coincides with its coordinate space whilst remains different for particular structure elements. This simultaneously both complicates and facilitates chemical reactions involving the tubes depending on a particular reaction goal. A summarized view on chemical reactivity of the tubes, presented in detail by the $N_{DA}$ maps in Figs. 4, 5, 7, 8, and 11 is given in Table 3. Shifting the activity to either cap or empty end regions depending on the tube shape and composition may be used in looking for practical ways of the tube chemical covalent modification.
2. Local additions of short-length addends (involving individual atoms, simple radical and so forth) to any SWCARBON NANOTUBE are the most favorable at open empty ends, both armchair and zigzag ones, and the latter somewhat more effective. Following these places in activity are end caps, defects in the tube sidewall, and sidewall itself.
3. Chemical reactivity of the open but chemically terminated ends of SWCARBON NANOTUBEs exceeds the one of sidewall only for tubes with zigzag ends.
4. Single local addition of long-length addends (polymers) will follow similar rules. However wrapping along the SWCARBON NANOTUBE sidewall will be more favorable due to a large number of local contacts on the way.
5. Chemical contacts of SWCARBON NANOTUBEs with spatially extended partners (surfaces of crystalline and amorphous solids, thin films, graphene sheets, etc) form an interface between the bodies the configuration of which depends on whether the tube is oriented normally to or parallel over the partner. In the latter case, a particular situation occurs when mono-atomic-layered graphene may act additionally as a cutting blade [62].
6. Addition reactions with participation of multi-walled carbon nanotubes will proceed depending on the target atoms involved. If the tubes empty open ends are main targets, the reaction will proceed as if one deals with an ensemble of individual SWCARBON NANOTUBEs. If sidewall becomes the main target the reaction output will depend on accessibility of inner tubes sidewall additionally to the outer one.

### 4.3. Comparison with experiment

Lack of experimental data for individual single-walled carbon nanotubes complicates the exact verification of the obtained data. However, there are some generalized observations which can be discussed in view of the performed computations.

1. Studies performed by Yates et al. [63] and Yates and Smalley et al. [64] can be attributed to the investigation of oxidatively cut SWCARBON NANOTUBE caps of ~1 nm in diameter thus revealing empty open ends interacting with primarily esters and quinones. Such oxidized SWCARBON NANOTUBEs have been assembled on a number of surfaces, including silver [65], highly oriented pyrolytic graphite [66], and silicon [67]. High coverage densities and orientation normal to the surface have been shown; the latter being suggestive of higher degrees of functionalization at the nanotube ends. The findings correlate well with calculated high reactivity of the SWCARBON NANOTUBE empty open ends [11].
2. Frequently, intrinsic defects on SWCARBON NANOTUBEs are supplemented by oxidative damage to the nanotubes framework by strong acids which leave holes functionalized with oxygenated groups such as carboxylic acid, ketone, alcohol, and ester group [68]. This and other studies (see reviews [37, 40, 69]) point to high chemical reactivity of the defects, which is in good agreement with the calculated data [11].
3. Attributing end caps of SWCARBON NANOTUBEs to the chemically active regions is widely accepted [35, 70]. However, as shown by calculations, this region is not always the most active since its activity can be overcome by a particular composition of open ends.
4. There was skepticism concerning the sidewall activity, which was considered much smaller with respect to that of fullerenes [35-46]. However, producing small diameter SWCARBON NANOTUBEs has removed the doubts opening the way to large scale hydrogenation [71], fluorination [72], amination [72], and a great number of other addition reactions [41, 73] involving SWCARBON NANOTUBEs sidewalls.

Therefore, available chemical data correlate well with predictions to be made on the basis of the computations described in Section 4.1. Particularly, the available data on the experimental study of hydrogenated SWCARBON NANOTUBEs [71] should be noted. As shown, a significant perturbation of SWCARBON NANOTUBEs structure under hydrogenation occurs. The finding seems to be understood on the basis of data [11] concerning the tube with both H-terminated open ends (see Fig. 8). The computations clearly highlight that attaching hydrogen atoms to the most active places of the tube causes a significant disturbance of its $N_{DA}$ map and, consequently, the tube structure which is spread over large region. Obviously, the more atoms are attached, the more drastic changes occur that is observed experimentally.

### 4.4. Electronic characteristics of single-walled carbon nanotubes

The largest set of data was obtained for (4,4) fragments which allowed presenting a summarized view on electronic properties of the tubes listed in Table 4.

1. According to the fragment energy, end-cap/H-terminated-open-end and H-terminated-open-end/H-terminated-open-end tubes are the most energetically stable among unilength fragments NT5-NT9.
2. Removing eight hydrogen terminators from end-cap/H-terminated-open-end tubes (NT1 and NT5) requires 465.7 and 486.3.kcal/mol in the case of shorter NT2 and longer NT6 tube, respectively. Supposing this energy is needed for the disruption of C-H bonds one obtains 58.2 and 60.8 kcal/mol (or 2.5 and 2.6 eV) per one bond that is in good consistence with both experimental [71] and calculated data [45, 46] estimating the energy of ~2.5eV for the formation of one C-H bond.
3. Substitution of eight terminators at the open end of NT1 fragment by the second cap in NT3 one requires 264.8 kcal/mol that is essentially less than needed for emptying the end.

**Table 4**. Basic electronic characteristics of fragments of (4,4) single-walled carbon nanotube [1] [11]

| *Fragments* | UBS HF singlet state | | | | | |
|---|---|---|---|---|---|---|
| | *Symmetry* | *ΔH, kcal/mol* | *D, D* | *I, eV* | *ε, eV* | $N_D$ |
| NT1 | $C_{2v}$ | 1182.60<br>1342.84[2] | 9.928 | 9.19 | 2.19 | 32.38 |
| NT2 | $C_2$ | 1648.34 | 0.440 | 9.71 | 3.16 | 39.59 |
| NT3 | $D_{2h}$ | 1447.39 | 0.029 | 9.81 | 2.45 | 33.35 |
| NT4 | $C_S$ | 1271.77 | 9.954 | 9.13 | 2.21 | 32.60 |
| NT5 | $C_{2v}$ | 1476.6 | 10.390 | 9.16 | 2.26 | 42.17 |
| NT6 | $C_2$ | 1962.91 | 0.428 | 9.71 | 3.14 | 50.47 |
| NT7 | $C_{4h}$ | 1271.42 | 0.003 | 8.20 | 2.38 | 37.96 |
| NT8 | $C_{4h}$ | 1689.58 | 10.990 | 9.19 | 2.92 | 47.36 |
| NT9 | $C_{2h}$ | 2136.90 | 0.225 | 9.66 | 3.04 | 54.90 |

1) *ΔH, D, I,* and *ε* present the heat of formation, dipole moment, ionization potential, and electron affinity, respectively.
2) Restricted Hartree-Fock data. Similar ~14% increasing in the energy value has been observed for all studied fragments when going from UBS HF to the restricted Hartree-Fock calculation scheme.

4. Emptying one open end of the H-terminated-open-end/H-terminated-open-end NT7 fragment costs 418.2 kcal/mol (52.3 kcal/mol per one C-H bond) while additional removing eight hydrogen terminators from the other end of NT8 fragment adds 447.3 kcal/mol (55.9 kcal/mol) to the energy cost. As seen, the obtained data for the end-cap/open-end tube and open-end/open-end one are well consistent.
5. All three end-cap/H-terminated-open-end tubes (NT1, NT4, and NT5) are polarized with a large dipole moment of ~10 D while the end-cap/empty-open-end (NT2, NT6) and end-cap/end-cap (NT3) tubes have a very low dipole moment, if any. Practically, this circumstance is very important when applying SWCARBON NANOTUBEs either to improve the characteristics of nonlinear optical devices based on liquid crystalline media [74, 75] or to design new hybrid materials based on SWCARBON NANOTUBEs and electron donor-acceptor nanocomposites [41].
6. Among open-end tubes, the H-terminated-open-end/empty-open-end (NT8) tube is the most polarized while H-terminated-open-end/H-terminated-open-end (NT7) and empty-open-end/empty-open-end (NT9) tubes have small dipole moments.
7. It is important to note the high level of donor-acceptor characteristics of the tubes. All tubes are characterized by not very high ionization potentials and high electron affinity. The characteristic value $I_D$-$\varepsilon_A$ is in interval of 7.4-5.9 eV, it meets the requirements of the formation of tightly coupled adducts involving two or more SWCARBON NANOTUBEs leading to their donor-acceptor-stimulated adhesion similarly to the dimerization of fullerene $C_{60}$ [76]. At the same time this explains a high acceptor ability of SWCARBON NANOTUBEs in numerous donor-acceptor nanocomposites [41].

Once related to single-walled carbon nanotubes of the (4,4) family, the obtained regularities can be nevertheless spread over other (n,n) and (m,0) tubes due to close similarity in their behavior exhibited in [11]. To sum up, the obtained results clearly show that the application of UBS HF for detailed quantitative characterization of both single-walled carbon nanotubes chemical reactivity and their electronic characteristics was quite informative and efficient.

### 4.5. Chemical reactivity of graphene

Low and homogeneous chemical reactivity of atoms through over a graphene sheet is usually expected by the predominant majority of scientists dealing with the graphene chemistry. However, as shown by UBS HF calculations [12, 30], it is not the case since the length of equilibrium C-C bonds of graphene exceeds 1.395 Å that is the upper limit when a complete covalent coupling between odd electrons occurs (See Section 3). The calculated

results for graphene sheets of different size (nanographens NGrs below) are listed in Table 5. Rectangular NGrs are nominated as ($n_a$. $n_z$) structures following [77]. Here $n_a$ and $n_z$ match the number of benzenoid units on the armchair and zigzag edges of the sheets, respectively. The ACS ($N_{DA}$) profile for NGr (15, 12) with hydrogen terminated edges presented in Fig.12a demonstrates a rather significant variation of the quantity over atoms due to a noticeable dispersion of the C-C bond lengths. Shown by computations, the equilibrium sheet structure is characterized by a remarkable varying of C-C bond lengths while the structure optimization in all cases starts with practically constant bond lengths through over the sheet with the C-C bond length of 1.43-1.42 Å. It should be noted that this variation is a direct consequence of taking effectively unpaired electrons into account. When the spin peculiarities are omitted and calculations are performed in the close-shell restricted Hartree-Fock and DFT approximations the bond length variation is absent.

As seen from the figure, the highest atomic chemical susceptibilities are characteristic of carbon atoms at the zigzag edges while those of the armchair edges are similar to the suptibility values of the sheet inner atoms and are comparable with the ones of fullerenes [5, 20] and SWCARBON NANOTUBEs sidewall [11, 29]. When hydrogen terminators are removed, the ACS profile over the sheet remains unchanged while $N_{DA}$ values on both zigzag and armchair edges grow significantly (Fig.12b) still conserving bigger values for zigzag edges.

Obtained results made allowance for the following conclusions concerning chemical reactivity of nanographenes [12, 30].

- Any chemical addend will be firstly attached to the graphene zigzag edges, both hydrogen terminated and empty;
- Slightly different by activity non-terminated armchair edges compete with zigzag ones;
- Chemical reactivity of inner atoms does not depend on the edge termination and is comparable with that of SWCARBON NANOTUBE sidewall and fullerenes thus providing a large range of addition reactions at the graphene surface.
- The disclosed chemical reactivity of both edges and inner atoms of graphene causes a particular two-mode pattern of the nanographene attaching to any spatially extended molecular object such as either carbon nanotube or substrate surface, namely, a normal mode and a tangent or parallel one.

Let us look at the results of the UBS DFT studies of nanogrphenes. First notification about peculiar edge states of graphene ribbons appeared as early as 1987 [78] but further extended study started about ten years later [79, 80]. Since that time three main directions of the peculiarity investigation have been shaped up that were focused on 1) edge states within band structure of graphene; 2) chemical reactivity and 3) magnetism of graphene's ribbon zigzag edges. The first topic lays mainly within the framework of the solid state theory concerning the formation of localized states caused by the breakage of translational symmetry in a certain direction that occurs when a graphene sheet is cut into graphene ribbons. This fundamental property was well disclosed computationally independently on the technique used [80, 81] and was approved experimentally [82, 83]. Two other topics are intimately connected with UBS DFT [57, 84-86] itself and demonstrate a spin-contaminated character of the obtained solutions.

The first UBS DFT examination of the chemical reaction between a hydrogen-terminated graphene ribbon and common radicals [84] disclosed *unpaired π electrons* (authors' nomination) distributed over zigzag edges in 0.14 *e* on each atom ($N_{DA}$ in terms of the current paper). The finding permitted the authors to make conclusion about open-shell character of the graphene singlet ground state of the ribbon as well as of special chemical reactivity of the atoms which leads to a partial radicalization of the species. The next authors' conclusion concerned nonedge ribbon carbon atoms, armchair atoms as well as carbon nanotube (presumably sidewall) atoms that show little or no radical character.

**Table 5.** Atomic chemical susceptibility of H-terminated nanographenes [12, 30]

| Nanographenes ($n_a$. $n_z$)[1] | $N_{DA}$, *e* | | |
|---|---|---|---|
| | Armchair edge | Central part | Zigzag edge |
| (15, 12)<br>(15, 12)[2] | 0.28-0.14<br>1.18-0.75 | 0.25-0.06<br>0.25-0.08 | 0.52-0.28<br>1.56-0.93 |
| (7, 7) | 0.27-0.18 | 0.24-0.12 | 0.41-0.28 |
| (5, 6) | 0.27-0.16 | 0.23-0.08 | 0.51-0.21 |

[1] Following [77], $n_a$ and $n_z$ match the numbers of benzenoid units on the armchair and zigzag ends of the sheets, respectively.
[2] After removing hydrogen terminators

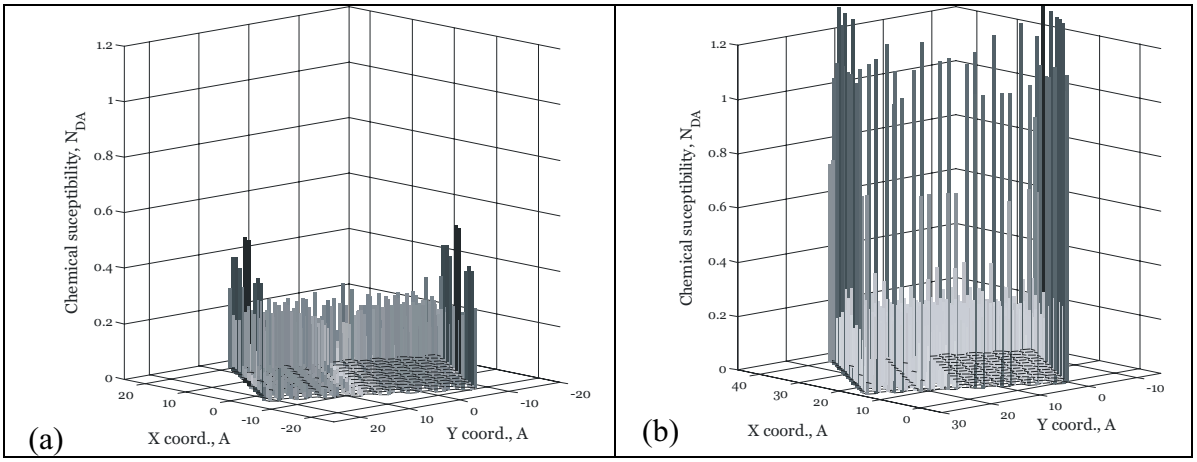


Figure 12. Distribution of atomic chemical susceptibility over atom of rectangular nanographene NGr (15,12) with hydrogen terminated (a) and empty (b) edges. UBS HF solution. Singlet state [12].

The cited UBS DFT results correlate with those of UBS HF [12, 30] in two points. Both approaches disclosed open-shell character of the ground singlet state of graphene and established the availability of effectively unpaired electrons. However, the numbers of effectively unpaired electrons differ by an order of magnitude that restricted the UBS DFT discussion of the chemical reactivity of graphene by zigzag edge atoms only. The fixation of the open-shell character of the graphene ground singlet state by both UBS techniques was obvious due to the single-determinant character of the wave functions in the two cases. The feature was revealed due to considerable weakening of the odd electron interaction in graphene caused by rather large C-C bond lengths. As for the magnitude of the unpaired odd ($\pi$) electrons numbers $N_{DA}$, it is difficult to discuss the DFT value since no indication of the way of its determination is presented. Its decreasing by one order of magnitude comparing to the UBS HF data might indicate a pressed-by-functional character of the UBS DFT calculations [15].The functional-dependent character of the UBS DFT solutions was thoroughly analyzed just recently [87, 88]. At any rate, the results clearly exhibited much lower sensitivity of the UBS DFT approach to chemical reactivity of atoms which can be imagined as lifting a zero reading level up to 0.2-0.3 *e* in Fig.12a and up to 1.1 *e* in Fig.12b, thereafter the fixation of values below the level becomes impossible.

The close-to-zero chemical reactivity of graphene inner atoms predicted by the UBS DFT calculations strongly contradicts to the active chemical adsorption of individual hydrogen and carbon atoms on graphene surface recently disclosed experimentally [89]. To the most extent, the chemical reactivity of inner atoms has been proven by the formation of a chemically-bound interface between a graphene layer and silicon dioxide over the course of the graphene sheet [90] as well as by producing a new particular one-atom-thick CH species named as graphane [91]. At the same time, the empirical observations are well consistent with the UBS HF data obtained in [12, 30].

A strong support in favor of the UBS HF data obtained was found in the recent many-body configurational interaction calculations of polyacenes [92]. Applying *ab initio* density matrix renormalization group (DMRG) algorithms, the authors highlighted the radical character of the acenes that is caused by the appearance of effectively unpaired electrons and that starts in naphthalene and strengthens when the acene size increases in full agreement with the UBS HF data for lower acenes disclosed previously [29]. Oppositely, UBS DFT approach rejected the radicalization in this case until the acene becomes quite long [93]. The DMRG approach permitted as well to determine the total number of effectively unpaired electrons $N_D$. When utilizing the algorithm for the quantity determination suggested in [18] and presented by Ex. (8) in Section 2.1, the authors obtained $N_D$ values that coincide with the relevant data obtained in the framework of the UBS HF approach based on the same algorithm [30] (see Table 6). The observed fitting of DMRG and UBS HF is undoubtedly a strong support in favor of the ability of UBS HF approach to highlight physical reality of a system of weakly interacting electrons. That is why one can accept the obtained data on chemical reactivity of graphene as quite reliable and use ACS values as quantified pointers for predicting chemical reactions and/or modifications to which graphene can be subjected. Thus, the disclosed reactivity of both graphene edge and inner atoms as well as a possible two-mode pattern of approaching nanographene sheet to a carbon nanotube permitted to suggest a number of peculiar graphene-nanotube composites [62, 94] whose appearance might be expected in the near future.

## 5. Magnetism of zigzag edged nanographenes

The phenomenon, predicted and studied computationally for graphene nanoribbons, is one of the hottest issue of the graphene science (enough to mention tens of papers presented on recently hold International conference on Nanotubes Science NT08 [95]). At the heart of the statement of the graphene magnetism are localized states whose flat bands are located in the vicinity of the Fermi level and whose peculiarities were attributed to zigzag edges [57, 78-80, 84, 85, 87, 88]. In numerous UBS DFT studies this fact was connected with the spin density on edge atoms. Computations were carried out in presumably Ψ-contaminated UBS DFT approximations following such a logical scheme: taking into account spins of edge atoms at the level of wave function; considering so-called antiferromagnetic (AFM) and ferromagnetic (FM) spin configurations with spin alignment up on one edge and down (up) on the other edge, respectively, or nonmagnetic configuration when up-down spin pairs are located at each edge, and performing calculations for these spin configurations. The obtained results have shown that 1) the antiferromagnetic configuration corresponds to the open-shell singlet ground state and is followed in stability by ferromagnetic and then nonmagnetic states; 2) the calculated spin density on edge atoms corresponds to the input spin configurations in all cases. It should be added that numerical results obtained in different studies differ from each other when different functionals were used under calculations.

However, the UBS DFT antiferromagnetic (singlet) state is as spin-contaminated as the UBS HF one and the availability of the spin density is just a strong confirmation of the contamination. Nevertheless, the presence of spin density at zigzag edge atoms was accepted as a decisive point in heralding magnetism of graphene ribbons after which the phenomenon was considered to be confirmed that gave rise to a big optimism towards the expectation of a number of exciting applications of the material, in spintronics for example [96].

Since spin density is a direct evidence of the solution spin-contamination, particularly for singlet state, it is worth comparing spin density data computed at the UBS DFT and UBS HF levels of the theory. The UBS HF spin density distribution over NGr (15,12) atoms with hydrogen-terminated and empty edges [12, 30] is demonstrated in Fig.13. As seen from the figure, the spin density is available at all atoms of the graphene sheet. In both cases, its summation over all atoms gives zero since the ground state is singlet. The spin density at zigzag edge atoms is the highest, even absolutely dominating when the edges are emptied.

**Table 6.** Total number of effectively unpaired electrons followed from Ex.(5)

| Molecules | $N_D$, *e* | |
|---|---|---|
| | UBS HF [30] | DMRG [92] |
| Benzene | 0 | – |
| Naphtalene | 1.48 | 1.95 |
| Anthracene | 3.00 | 3.00 |
| Tetracene | 4.32 | 4.00 |
| Pentacene | 5.54 | 5.20 |

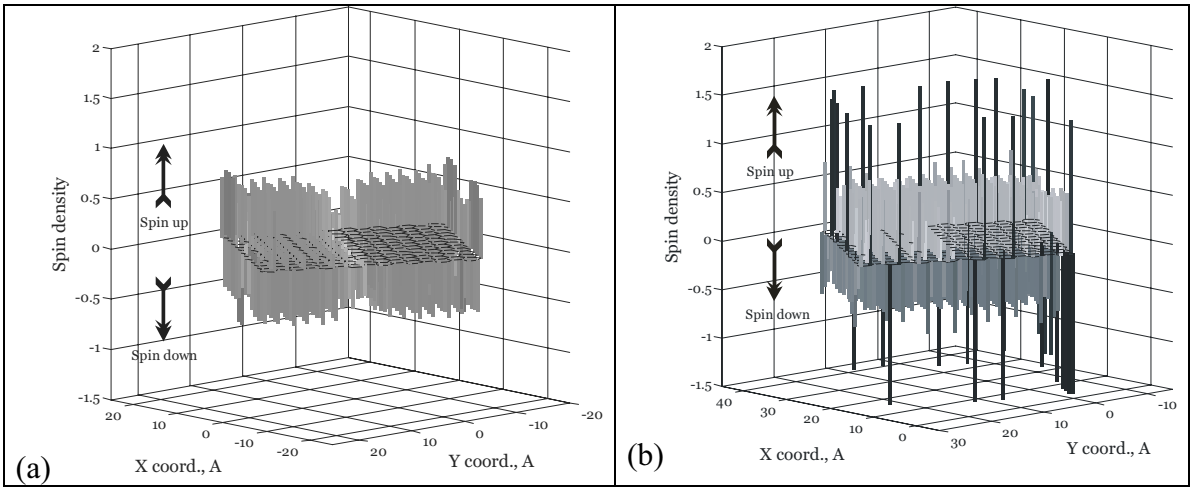


Figure 13. Distribution of spin density over atom of rectangular nanographene NGr (15,12) with hydrogen terminated (a) and empty (b) edges. UBS HF solution. Singlet state [12].

Oppositely to the case, UBS DFT data are related to zigzag edge atoms only and spin density absolute values vary from 0.26 to 0.47 when the local density functional is replaced by the screen exchange hybrid density functional [87]. To see only these atoms in Fig.13 means lifting the zero reading level up (down) to ~±0.4 in the first case and to ±1.3 in the second one, that, by other words, means lowering sensitivity in recording the density values. This is the same situation caused by the pressed-by-functional character of the UBS DFT solution that was discussed for the atomic chemical susceptibility profiles in the previous section.

It should be noted that the UBS HF spin density on zigzag edge is distributed quite peculiarly not following the above mentioned up- and down-edge antiferromagnetic configuration assumed for the ground state by UBS DFT. Remaining that spin density value is sensitive to the C-C bond length, it becomes clear why varying the latter produces variation in the density distribution as well. Therefore, the UBS HF data differ from those of UBS DFT both qualitatively and quantitatively not supporting a ranged configuration of spins on zigzag edge atoms only. At the same time, the UBS HF data well correlate with so far the only many-body configuration interaction calculations of the edge states of graphene [88]. The latter infer that although the electrons have the tendency to accumulate at the edges, the spin distribution is quite irregular so that a net spin polarization of the edges is highly improbable. Therefore, as in the case of the chemical reactivity of graphene discussed in the previous Section, many-body configurational interaction calculations supports the ability of UBS HF to highlight main physical features of weakly interacting electrons.

Coming back to magnetism of graphene ribbons, let us stand from the fact that the real ground state of the object is pure-spin singlet. This means that the real spin density at each atom is zero. We can nevertheless discuss the possibility of the magnetic behavior of the object however not from the spin density viewpoint but addressing the energy difference between states of different spin multiplicity as was discussed in Section 2.2.

An attempt to go outside the spin-density concept at the UBS DFT level was made in [87]. This time the main attention was concentrated on the difference in position of singlet and high spin (mainly triplet) states of graphene nanoribbons, thus implicitly appealing to the $J$ value. However, as said in Section 2.2, the magnetic coupling constant $J$ should be attributed to the difference of pure-spin states energies while the UBS DFT states under discussion are spin-mixed so that their energies do not correspond to those of pure-spin states that makes the authors conclusions quite uncertain.

Oppositely to UBS DFT, UBS HF offers a straightforward way in determining pure spin states [8]. Computed accordingly to Eq. (10) $E_{S=0}^{PS}$ as well as $E_{S=0}^{UBS\ \ HF}$, and $J$ values related to the studied nanographenes are listed in Table 7. As seen from the table, the ground state of all species is singlet so that a question arises if the magnetization of singlet-ground-state object is possible. As discussed in [26], the phenomenon may occur as a consequence of mixing the state with those of high multiplicity following, say, to the van Fleck mixing promoted by applied magnetic field [97]. Since the effect appears in the first-order perturbation theory, it depends on $J$ that determines the energy differences in denominators. Consequently, $J$ should be small to provide noticeable magnetization. Obviously, singlet-triplet mixing is the most influent. As follows from Table 7, the energy gap to the nearest triplet state for the studied nanographenes constitutes 1-4 kcal/mol. The value is large to provide a noticeable magnetization of these molecular magnets [27]. However, the value gradually decreases when the number of odd electrons increases. The behavior is similar to that obtained for fullerene oligomers [28] that led to the suggestion of a scaly mechanism of nanostructured solid state magnetism of the polymerized fullerene $C_{60}$.

In view of this idea, it was possible to estimate how large should be nanographene to provide a noticeable magnetization [12, 30]. As known [27], molecular magnetism can be fixed at $J$ value of $10^{-2}$-$10^{-3}$ kcal/mol or less. Basing on the data presented in Table 7 and supposing the quantity to be inversely proportional to the number of odd electrons, $N$ should be $\sim 10^5$. In rectangular nanographenes $N$ coincides with the number of carbon atoms that is determined as [77]

$$N = 2\left(n_\alpha n_z + n_\alpha + n_z\right). \qquad (15)$$

To fit the needed $N$ value, the indices $n_\alpha$ and $n_z$ should be of hundreds that leads to linear sizes of nanographenes of a few *nm*. The estimation is rather approximate but it nevertheless correlates well with experimental observations of the magnetization of activated carbon fibers consisting of nanographite domains of 3-5 nm in size [98, 99].

## 6. Siliceous graphene - silicene

Silicon-based nanotechnology has attracted the hottest attention since the first steps of nanotechnology to become a reality. Silicon-based nanoelectronics seemed an obvious extension of conventional silicon microtechnology. The first peak of interest was connected with the adventure of STM “atom writing” on the silicon crystal surfaces. A controllable deposition and/or extraction of silicon atoms from the surfaces seemed to open a direct way to design electronic nanochips of any kind. However, the works, pioneered by Prof.M.Aono and his team in Japan as well as by other groups throughout the world, met serious difficulties on the way that showed unexpected complications connected with the surfaces properties. Thus, the most promising Si(111)(7x7) surface occurred to be metallic and magnetic in contrast to semiconductive and non-magnetic bulk silicon. Silicon nanoelectronics did not meet with success at that time, although undertaken efforts stimulated a large realm of silicon surface science and the current extended materials nanoarchitechtonics (see projects of the International Center for Materials Nanoarchitectonics at NIMS in Japan).

**Table 7.** Electronic characteristics of nanographenes[1] in *kcal/mol* [30]

| Nanographenes[2] | The number of "magnetic"(odd) electrons | $E_{S=0}^{UBS\ \ HF}$ | $J$ | $E_{S=0}^{PS}$ | Singlet-triplet gap[3] |
|---|---|---|---|---|---|
| (15, 12) | 400 | 1426.14 | -0.42 | 1342.14 | 0.84 |
| (7, 7) | 120 | 508.69 | -1.35 | 427.69 | 2.70 |
| (5, 6) | 78 | 341.01 | -2.01 | 262.72 | 4.02 |

[1] Tabulated energies $E_{S=0}^{UBS\ \ HF}$ and $E_{S=0}^{PS}$ correspond to the heats of formation of the relevant states.

[2] Nomenclature of nanographenes see in Footnote 1 to Table 5.

[3] For pure-spin states the singlet-triplet gap $E_{S=1}^{PS} - E_{S=0}^{PS} = -2J$ [8].

The next pulse of interest is being observed nowadays. It has been stimulated by extreme expectations connected with graphenium nanoprocessors. However, despite the reigning optimism about the devices, the graphene discoverers pointed out that the processors appearance was unlikely for the next 20 years [100] since replacement of the current silicon electronics technology is a tough hurdle. And again a compatibility of silicon-based nanoelectronics with the conventional one has stressed attention to the question if carboneous graphene can be substituted by its siliceous counterpart named as silicene. Meeting the demands, the December08 internet news has brought information on "epitaxial growth of graphene-like silicon nanoribbons" [101]. The report, based on the hexagon-patterned accommodation of silicon atoms adsorbed on the [110] Ag surface, has heralded the silicene manifestation and is full of exciting applications to be expected.

However, under detailed examination [102], the situation does not seem so transparent and promising. To clear the said let us specify basic terms. First, we have to make clear what is implied under the term *silicene*. If any hexagon-packed structure of silicon atoms can be named silicene, then it has been known for long ago as, say, widely known silicon nanowires. However, four valence electrons of each silicon atoms form $sp^3$ configuration and participate in the formation of four chemical bonds in this case so that nobody could pretend to look for a similarity between these species and carboneous graphene. Therefore, not hexagon packing itself but a mono-atom-thick hexagon structure that dictates $sp^2$ configuration for atom valence electrons with the lack of one neighbor for each silicon atom meets requirements of comparison of silicene to graphene. Obviously, similar hexagon patterns should form the ground for silicon nanotubes. Only under these conditions graphene and silicene, as well as carboneous and siliceous nanotubes can be considered on the same basis.

As for theoretical consideration, performed computations of silicene [103] and silicon nanotubes [104-106] meet the requirement completely. Oppositely, experimental reports are full of appealing to silicon nanotubes (see a brief review [107]) and silicene [101] (in the first announcement of the finding observed [108], the latter was attributed to silicon nanowires) in spite of the evident $sp^3$configuration of silicon atoms in the structures observed. The fact was accepted by the experimentalists themselves. But a temptation to disclose silicon nanotubes and silicene seems to be so strong that the difference in the electron configuration is simply omitted. A detailed analysis of the available experimental data shows that silicon structures that can be compared to carbon nanotubes and graphene have not yet been observed. If remember that fullerene $Si_{60}$ has not been produced as well we have to accept the availability of a serious reason that causes so drastic difference between carboneous and siliceous analogues.

The problem is not new and is rooted deeply so that "…A comparison of the chemistry of tetravalent carbon and silicon reveals such gross differences that the pitfalls of casual analogies should be apparent" [109]. Enough to remind that there is no either silicoethylene or silicobenzene as well as other aromatic-like molecules. A widely spread standard statement

that "silicon does not like $sp^2$ configuration" just postulates the fact but does not explain the reason of such behavior. A real reason has been disclosed for the first time when answering question why fullerene $Si_{60}$ does not exist [20, 110]. The answer addressed changing in electron interaction for the two species when their electron configurations were transformed from $sp^3$ to $sp^2$-type. The interaction of two odd electrons, which are formed under the $sp^3$ – to- $sp^2$ transformation of any interatomic bond, depends on the corresponding distance $R_{\text{int}}$ that is ~1.5 times larger for Si-Si chemical bonds with respect to the C-C ones. As was shown in Section 3, generally, the distance $R_{\text{int}} = 1.4A$ is critical for these electrons to be covalently coupled [5]. Above the distance the electrons become effectively unpaired, therewith the more the larger the distance. In the case of graphene, distances between two odd electrons fill the interval 1.39-1.43A. Evidently, only parts of C-C bonds exceed the limit value that causes partial exclusion of odd electrons from the covalent coupling which makes the molecular species partially radicalized as discussed in Sections 4 and 5. The radicalization is rather weak since only ~10% of all odd electrons (equal to the number of atoms $N$) are unpaired. Oppositely to the case, $R_{\text{int}}$ in siliceous species is of 2.3-2.4A that causes a complete unpairing of all odd electrons so that all siliceous species with expected $sp^2$configuration should be many-fold radicals.

The application of UBS HF approach to the problem made these expectations evident [102]. Table 8 lists calculation results of the total number of unpaired electrons $N_D$ as well as a set of energetic parameters for a number of siliceous $sp^2$-configured species shown in Fig. 14. As seen from the table, there is a drastic lowering of the total energy of the species, constituting about 20-30% of the largest values, when close-shell restricted Hartree-Fock scheme is substituted by open-shell UBS HF. Large numbers of effectively unpaired electrons $N_D$ for all species indicate highly spin-contaminated character of their singlet UBS HF state. Following the procedure suggested by Noodleman [8], the energy of the singlet pure-spin states was determined according to (10). Thus obtained energies $E_{S=0}^{PS}$ are given in the table. As should be expected, the energy is lower than both $E_{S=0}^{RHF}$ and $E_{S=0}^{UBS\ HF}$, while rather close to the latter.

It should be emphasized that the numbers of effectively unpaired electrons $N_D$ listed in the table coincide quite well with the total numbers of silicon atoms ($N$) in all cases when the edges of the considered siliceous species are terminated by hydrogen atoms and exceed $N$ by the number of two-neighbor atoms ($N_2$) when hydrogen terminators are taken off from either tubes ends or silicene edges. The finding exhibits that silicon fullerene as well as silicon nanotubes and silicene are many-fold radicals and cannot exist under ambient conditions. Important to note that no suitable passivation should be expected to provide the species stabilization since the passivation should be absolutely total that will result in the transformation of all $sp^2$-silicon atoms to the $sp^3$-ones. That is why one observes $sp^3$- silicon nanowires instead of $sp^2$-SiNTs [107] as well as $sp^3$-accommodated silicon atom adsorption layers on the (111) Ag surface instead of $sp^2$-silicene strips [101, 108].

Optimism expressed in theoretical papers where fullerene $Si_{60}$ [111, 112], silicon nanotubes [104-106], and silicene [103] were considered, is mainly due to that the calculations were performed in the close-shell approximation (similar to RHF) so that the problem concerning weak interacting odd electrons was not taken into account.

## 7. Conclusion

The basic problem of weak interaction between odd electrons in carboneous species is considered within the framework of the broken spin-symmetry single-determinant approach. The modern implementations of the approach in the form of either unrestricted Hartree-Fock

**Table 8.** Energies[1] in *kcal/mol* and the number of effectively unpaired electrons in $sp^2$-configured siliceous species (see Fig.14) [102]

| Species | $N(N_2^2)$ | $E_{S=0}^{RHF}$ | $E_{S=0}^{UBS\ HF}$ | $E_{S=0}^{PS}$ | $N_D$ |
|---|---|---|---|---|---|
| I | 2 | 54,50 | 48,95 | 39,02 | 0.88 |
| II | 6 | 144,51 | 121,25 | 108,67 | 2.68 |
| III | 60 | 1295,99 | 1013,30 | 996,64 | 62.48 |
| IV a | 96 ($24^2$) | 2530,19 | 1770,91 | 1749,56 | 128 |
| IV b | 96 | 1943,14 | 1527,77 | 1505,48 | 95,7 |
| V a | 100 ($20^2$) | 2827,73 | 1973,67 | 1958,54 | 115,05 |
| V b | 100 | 2119,60 | 1580,77 | 1559,64 | 100,12 |
| VI a | 60 ($22^2$) | 1950,20 | 1359,44 | 1346,68 | 75,7 |
| VI b | 60 | 1253,39 | 1001,27 | 972,12 | 54,04 |

[1)] Tabulated energies $E_{S=0}^{RHF}$, $E_{S=0}^{UBS\ HF}$, and $E_{S=0}^{PS}$ correspond to the heats of formation of the relevant states.

[2)] Included number of two-neighbor edge silicon atoms

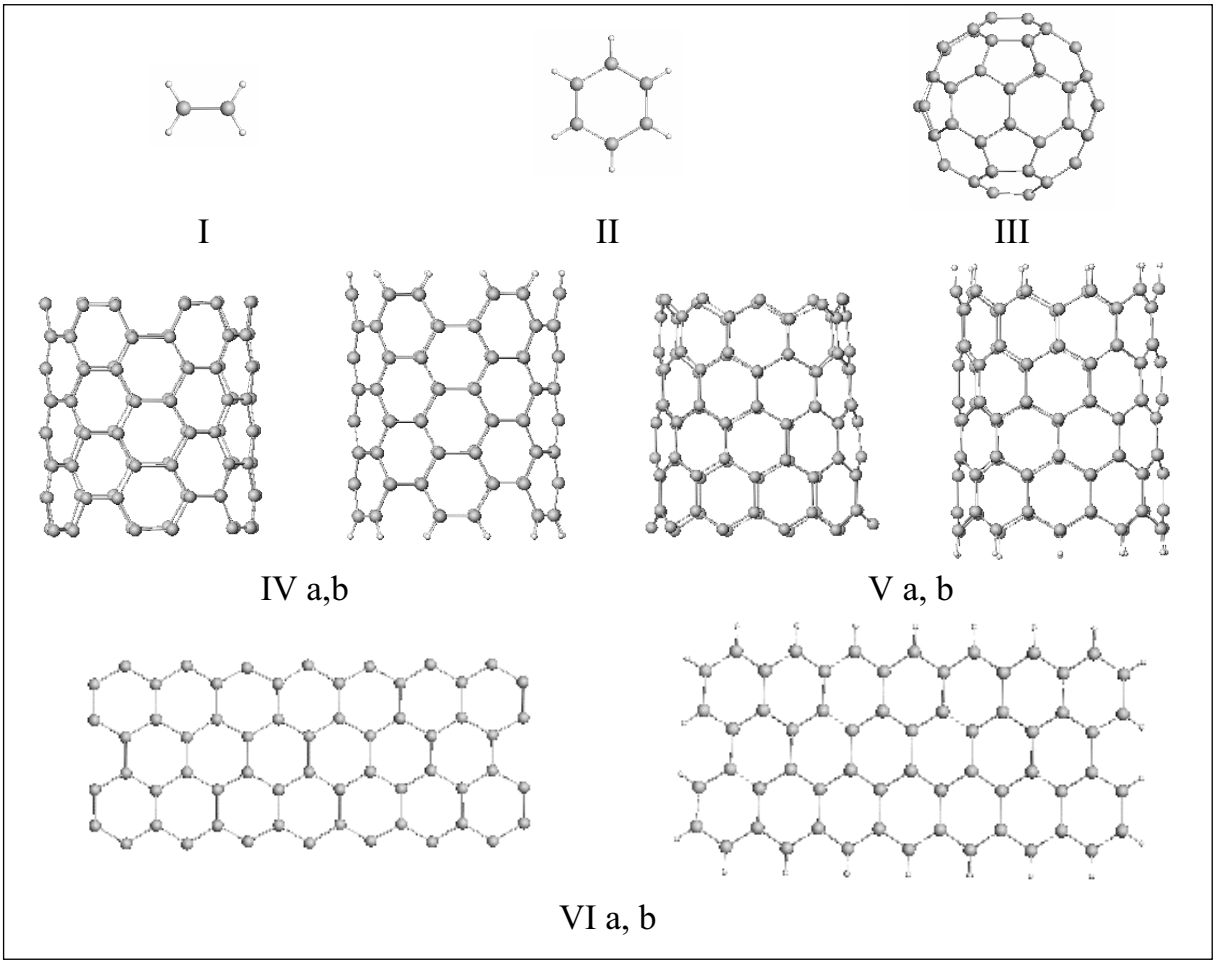


Figure 14. Equilibrated structures of $sp^2$-configured siliceous species, UBS HF, singlet state [102]: I- silicoethylene; II- silicobenzene; III- silicofullerene $Si_{60}$; IV- fragments of (6,6) silicon nanotube with empty (a) and hydrogen-terminated (b) end atoms; V- the same but for (10,0) silicon nanotube; VI- (3, 7) silicene sheet with empty (a) and hydrogen-terminated (b) edges.

scheme (UBS HF) or spin-polarized DFT (UBS DFT) were discussed with particular attention to the applicability of spin-contaminated solutions of both techniques for the description of electronic properties of the species. As for carbon nanotubes and graphene, the UBS DFT

applications generally reveal the open-shell character of the singlet state of the object and manifest an extra spin density concentrated on zigzag edge atoms. Similarly, the UBS HF approach supports these findings but exhibits the extra spin density not only on zigzag edge atoms but on all atoms of the species. This very peculiarity permits to quantitatively describe the odd electron behavior via both enhanced chemical reactivity and magnetism. The former is presented in terms of a quantified atomic chemical susceptibility that is continuously distributed over all atoms with the value similar to that of fullerenes and exceeds the latter at end atoms of carbon naotubes as well as edge atoms of graphene. The UBS HF calculations highlighted as well that magnetic response of graphene is provided by a collective action of all odd electrons and is size-dependent. The relative magnetic coupling constant $J$ decreases when the sheet size increases and $J$ approaches the limit value of $10^{-2}$-$10^{-3}$ kcal/mol, needed for the object magnetization to be recorded, when the sheet size is of a few *nm* that is well consistent with experimental findings.

A common view on both chemical reactivity and magnetism of fullerenes, carbon nanotubes, and graphene, physically clear and transparent, witnesses the internal self-consistency of the UBS HF approach and exhibits its high ability to quantitatively describe practically important consequences of weak interaction between odd electrons. The statement is well supported by a deep coherency of the obtained UBS HF results with those followed from the application of many-body configurational interaction calculation schemes to polyacenes and graphene. Applied to silicene and other $sp^2$-configures siliceous species, the approach discloses a complete unpairing of odd electrons that transforms the species into many-fold radicals and makes the producing of the substance absolutely impossible.

## Bibliography


1. *Hoffman R.* Interaction of orbitals through space and through bonds // Accounts Chem.Res. 1971, **4**, 1.
2. *Salem L., Rowland C.* The electronic properties of diradicals // Angew.Chem. Intern Edit. 1972, **11**, 92.
3. *Sheka E.F.* Odd electrons in molecular Chemistry, surface science, and solid state magnetism // Int.Journ.Quant.Chem. 2007, **107**, 2935.
4. *Illas F., Moreira I. de P.R., de Graaf C., Barone V*. Magnetic coupling in biradicals, binuclear complexes and wide-gap insolators; a survey of ab initio function and density functional theory approaches // Theor. Chem. Acc. 2000, **104**, 265.
5. *Sheka E.F.* Chemical susceptibility of sullerenes in siew of Hartree-Fock spproach // Int.Journ.Quant.Chem. 2007, **107**, 2803.
6. *Davidson E.R., Clark A.E.* Analysis of wave functions for open-shell molecules // Phys.Chem. Chem.Phys. 2007, **9**, 1881.
7. *Sadoc I., Boer, R., de Graaf, C.* Role of charge transfer configuration in $LaMnO_3$, $CaMnO_3$, and $CaFeO_3$ // J.Chem.Phys. 2006, **126**, 134709.
8. *Noodleman L.* Valence bond description of antiferromagnetic coupling in transition metal dimmers // J. Chem Phys. 1981, **74**, 5737.
9. *Pople J.A., Nesbet R.K.* Self-consistent orbitals for radicals // J.Chem.Phys. 1954, **22,** 571.
10. *von Barth U., Hedin L.* // J.Phys. C 1972, **5**, 1629.
11. *Sheka E.F., Chernozatonskii L.A.* Broken symmetry approach and chemical susceptibility of carbon nanotubes // Int.Journ.Quant.Chem. 2009, **109**, 12.
12. *Sheka E.F., Chernozatonskii L.A.* Chemical reactivity and magnetism of graphene // 2009, arXiv: 0901.3757v1, http://arxiv.org/abs/0901.3757 23 Jan 2009.
13. *McWeeny R.* In Electron Density, Density Matrix and Density Functional Theory, 14. Gidopoulos, N.; Wilson, S., Eds.; Kluwer: Dodrecht, 2003; p. 97. Series: Progress in Theoretical Chemistry and Physics.
14. *Kaplan I.* Problems in DFT with the total spin and degenerate states // Int.Journ.Quant.Chem. 2007, **107**, 2595.
15. *Adamo C., Barone V., Bencini A., Broer R., Filatov M., Harrison N.M., Illas F., Malrieu J.P., Moreira I. de P.R.* Comment on "About the calculation of exchange coupling constants using density-functional theory: The role of the self-interaction error" // [J. Chem. Phys. **123**, 164110 (2005)], Journ. Chem.Phys. 2006, **124**, 107101.
16. *Löwdin P.O*. Quantum Theory of Many-Particle Systems. III. Extension of the Hartree-Fock Scheme to Include Degenerate Systems and Correlation Effects // Phys.Rev. 1955, **97**, 1509.

17. *Löwdin P.O*. Quantum Theory of Many-Particle Systems // Adv.Chem.Phys. 1969, **14**, 283.
18. *Takatsuka K., Fueno T., Yamaguchi K.* Distribution of odd electrons in ground-state molecules // Theor.Chim.Acta. 1978, **48**, 175.
19. *Nagao H., Nishino M., Shigeta Y., Soda T., Kitagawa Y., Onishi T., Yosioka Y., Yamagucj K.* Theoretical studies on effective spin interactions, spin alignments and macroscopic spin tunneling in polynuclear manganese and related complexes and their mesoscopic clusters // Coord. Chem. Rev. 2000, **198**, 265.
20. *Sheka E.F., Zayets V.A.* The radical nature of fullerene and its chemical activity, Russ // Journ.Phys.Chem. 2005, **79**, 2009.
21. *Caballol R., Castell O., Illas F., Moreira I. de P.R., Malrieu J.P.* Remarks on the proper use of the, broken symmetry approach to magnetic coupling // J. Phys. Chem, 1997, **101A**, 7860.
22. *Noodleman L., Davidson E.* Ligand spin polarization and antiferromagnetic coupling in transition metal dimmers // Chem.Phys. 1986, **109**, 1311.
23. *Dai D., Whangbo M.-H.* Spin-Hamiltonian and density functional theory descriptions of spin exchange interactions // J.Chem.Phys. 2001, **114**, 2887.
24. *Seo D.-K.* Density functional perturbational orbital theory of spin polarization in electronic systems. II. Transition metal dimer complexes // J. Chem. Phys. 2007, **127**, 184103.
25. *Han W.-C., Noodelman L.* Structural model studies for the high-valent intermediate Q of methane monooxygenase from broken-symmetry density functional calculations // Inorg, Chim.Acta 2008, **361**, 973.
26. *Zvezdin A.K., Matveev V.M., Mukhin A.A. et al.* Redkozemeljnyje iony v magnito-uporjadochennykh kristallakh (Russian) (Rear Earth Ions in Magnetically Ordered Crystals) // Nauka, M., 1985.
27. *Kahn O.* Molecular Magnetism // VCH, New York, 1993.
28. *Sheka E.F., Zayets V.A., Ginzburg I.Ya.* Nanostructural magnetism of polymeric fullerene crystals // JETP 2006, **103**, 728.
29. *Sheka E.F., Chernozatonskii L.A.* Bond length effect on odd electrons Behavior in Single-walled Carbon nanotubes // J.Phys.Chem.C 2007, **111**, 10771.
30. *Sheka E.F., Chernozatonskii L.A.* Chemical reactivity and magnetism of graphene // Int. Journ. Quant. Chem, 2009 (in press)
31. *Bauernschmitt R., Ahlrichs R*. Stability analysis for solutions of the closed shell Kohn–Sham equation // J.Chem.Phys. 1996, **104**, 9047.
32. *Tasis T., Tagmatarchis N., Bianco N., Prato M.* Chemistry of carbon nanotubes // Chem.Rev. 2006, **106**, 1105.
33. *Meyer R.R., Sloan J., Dunin-Borkowski R.E., Kirkland A.I., Novotny M.C., Baily S.R., Hutchison J.L., Green M.L.H.* Discrete atom imaging of one-dimensional crystals formed within single-walled carbon nanotubes // Science 2000, **289**, 1324.
34. *Mickelson E.T., Huffman C.B., Rinzler A.G., Smalley R.E., Hauge R.H., Margrave J.L.* Fluorination of single-wall carbon nanotubes // Chem Phys. Lett. 1998, **296**, 188.
35. *Hirsh A*. Principles of fullerene reactivity // Top.Curr.Chem. 1999, **199**, 1.
36. *Niyogi S., Hamon M.A., Hu H., Zhao B., Bhomik P., Sen R., Itkis M.E., Haddon R.C.* Chemistry of single-walled carbon nanotubes // Acc.Chem Res. 2002, **35**, 1105.
37. *Bahr J.L., Tour J.M.* Covalent chemistry of single-wall carbon nanotubes // J.Mater.Chem. 2002, **12**, 1952.
38. *Strano M.S., Dyke C.A., Usrey M.I., Barone P.W., Allen M.J., Shan H., Kittrell C., Hauge R.H., Tour J.M., Smalley R.E.* Electronic Structure control of single-walled carbon nanotube functionalization // Science 2003, **301**, 1519.
39. *Dyke C.A., Tour J.M.* Covalent functionalization of single-walled carbon nanotubes for materials applications // J. Phys. Chem. 2004, **108A**, 11151.
40. *Banerjee S., Hemray-Benny T., Wong S.S.* Covalent surface chemistry of single-walled carbon nanotubes // Adv. Mater. 2005, **17**, 17.
41. *Guldi D.M., Rahman G.M.A., Zerbetto F., Prato M.* Carbon nanotubes in electron donor-acceptor nanocomposites // Acc.Chem.Res. 2005, **38**, 871.
42. *Herrero A., Prato M.* Recent advances in the covalent functionalization of carbon nanotubes // Mol.Cryst.& Liq.Cryst. 2008, **483**, 21.
43. *Chen Z.F. Thiel W., Hirsch A.* Reactivity of the convex and concave surfaces of single-walled carbon Nanotubes (SWCNTs) towards Addition Reactions: Dependence on the carbon-atom pyramidalization // Chemphyschem 2003, **4**, 93.
44. *Chen Z.F., Nagase S., Hirsch A., Haddon R.C., Thiel W*. Side-wall opening of single-walled carbon nanotubes (SWCNTs) by chemical modification: A critical theoretical study // Angew. Chem. Int. Ed. 2004, **43**, 1552.
45. ***Yildirim T., Gьlseren O.,*** *Ciraci S.* Exohydrogenated single-wall carbon nanotubes // Phys. Rev. B 2001, **64**, 075404.
46. ***Gьlseren*** *O., Yildirim T., Ciraci S.* Effects of hydrogen adsorption on single-wall carbon nanotubes: Metallic hydrogen decoration // Phys. Rev. B 2002, **66,** 121401.
47. *Choi W.I., Park S., Kim T-E,. Park N., Lee K-R., Ihm J., Han S.* Band-gap sensitive adsorption of fluorine molecules on sidewalls of carbon nanotubes: an ab initio study // Nanotechnology 2006, **17**, 5862.

48. *Mercury F., Sgamelotti A., Valentini L., Armentano I., Kenny J.M.* Vacancy-induced chemisorption of $NO_2$ on carbon nanotubes: A combined theoretical and experimental study // J. Phys.Chem.B, 2005, **109**, 13175.
49. *Mercury F., Sgamelotti A.* Functionalization of carbon nanotubes with Vaska's complex: A theoretical approach // J.Phys.Chem.B, 2006, **110**, 15291.
50. *Mercury F., Sgamelotti A.* Theoretical investigations on the functionalization of carbon nanotubes // Inorg.Chim.Acta 2007, **360**, 785.
51. *Lee Y-S., Marzari N.* Cycloaddition functionalizations to preserve or control the conductance of carbon nanotubes // Phys.Rev.Lett. 2006, **97**, 116801.
52. *Lee Y-S., Marzari N.* Cycloadditions to control bond breaking in naphthalenes, fullerenes, and carbon nanotubes: A first-principles study // J.Phys.Chem.C 2008, **112**, 4480.
53. *Zhao, J-x, Ding, Y-h.* Chemical functionalization of single-walled carbon nanotubes (SWNTs) by aryl groups: A density functional theory study // J.Phys.Chem. 2008, **112 C**, 13141.
54. *Haddon R.C.* Chemistry of the fullerenes: The manifestation of strain in a class of continuous aromatic molecules // Science 1993, **261**, 1545.
55. *Chen Y., Haddon R.C., Fang S., Rao A.M., Eklund P.C., Lee W.H., Dickey E.C., Grulkem E.A., Pendergrass J.C., Chavan A., Haley B.E., Smalley R.E.* Chemical attachment of organic functional groups to a single-walled carbon nanotube material // J.Mater.Res. 1998, **13**, 2423.
56. *Hammon M.A., Itkis M.E., Niyougi S., Alvarez T., Kuper C., Menon M, Haddon R.C.* Effect of rehybridization on the electronic structure of single-walled carbon nanotubes // J.Am.Chem.Soc. 2001, **123**, 11292.
57. *Chen Z., Jiang D., Lu X., Bettinger H.F., Dai S., Schleyer P.R., Houk K.N.* Open-shell singlet character of cyclacene and short zigzag nanotubes // Org. Lett. 2007, **9**, 5449.
58. *Zayets V.A.* CLUSTER-Z1: Quantum-Chemical Software for Calculations in the s,p-Basis" // Institute of Surface Chemistry, Nat. Ac.Sci. of Ukraine, Kiev, 1990.
59. *Wiberg K.B.* Application of the pople-santry-segal CNDO method to the cyclopropylcarbinyl and cyclobutyl cation and to bicyclobutane // Tetrahedron 1968, **24**, 1083.
60. *Semenov S.G.* In Evolution of the Valence Doctrine (in Russian) // Khimia, M., 1977, 148.
61. *Hersam M.C.* Progress towards monodisperse single-walled carbon nanotubes // Nature Nanotech. 2008, **3**, 387.
62. *Sheka E.F., Chernozatonskii L.A.* Graphene-carbon nanotube composites // 2009, arXiv:0901.3624v1, http://arxiv.org/abs/0901.3624 22 Jan 2009
63. *Mawhinney D.B., Naumenko V., Kuznetsova A., Yates J.T., Jr.* Infrared spectral evidence for the etching of carbon nanotubes: Ozone oxidation at 298 K // J.Am.Chem.Soc. 2000, **122**, 2383.
64. *Mawhinney D.B., Naumenko V., Kuznetsova A., Yates J.T., Jr., Liu J., Smalley R.E.* Surface defect site density on single walled carbon nanotubes by titration // Chem.Phys.Lett. 2000, **324**, 213.
65. *Wu B., Zhang J., Wei Z., Cai S., Liu Z.* Chemical alignment of oxidatively shortened single-walled carbon nanotubes on silver surface // J.Phys.Chem. B 2001, **105**, 5075.
66. *Yanagi H., Sawada E., Manivannan A., Nagahara L.A.* Self-orientation of short single-walled carbon nanotubes deposited on graphite // Appl.Phys.Lett. 2001, **78**, 1355.
67. *Chattopadhyay D., Galeska I., Papadimitrakopoulos F.* Metal-assisted organization of shortened carbon nanotubes in monolayer and multilayer forest assemblies // J. Am. Chem. Soc. 2001, **123**, 9451.
68. *Chen J., Hamon M.A., Hu H., Chen Y., Rao A.M., Eklund P.C., Haddon R.C.* Solution properties of single-walled carbon nanotubes // Science, 1998, **282**, 95.
69. *Khabashesku V.N., Bilups W.E., Margrave J.L.* // Acc.Chem.Res. 2002, **35**, 1087.
70. *Rakov E.* Chemistry of carbon nanotubes in Nanomaterial Handbook // Gogotsi Y. (Ed.), Taylor&Francis, Boca Raton, London, New York, 2006, 105-176.
71. *Nikitin A., Ogasawara H., Mann D., Denecke R,. Zhang Z., Dai H., Cho K., Nilsson A.* Hydrogenation of single-walled carbon nanotubes // Phys.Rev.Lett. 2005, **95**, 225507.
72. *Tasis D., Tagmatarchis N., Georgakilas V., Prato M.* Soluble carbon nanotubes // Chem-Eur.J. 2003, **9**, 4000.
73. *Dyke C.A. Tour J.M.* Overcoming the insolubility of carbon nanotubes through high degrees of sidewall functionalization // Chem.- Eur.J. 2004, **10,** 813.
74. *Vivien L., Riehl D., Hashe F., Anglaret E.* Nonlinear scattering origin in carbon nanotube suspensions // J. Nonlinear Optical Physics & Materials. 2000, **9**, 297.
75. *Shulev V.A., Filippov A.K., Kamanina N.V.* Laser-induced processes in the IR range in nanocomposites with fullerenes and carbon nanotubes // Techn.Phys.Lett. 2006, **32**, 694.
76. *Sheka E.F.* Donor-acceptor interaction and fullerene $C_{60}$ dimerization // Chem.Phys.Lett. 2007, **438**, 119.
77. *Gao X., Zhou Z., Zhao Y., Nagase S., Zhang S.B., Chen Z.* Comparative study of carbon and BN nanographenes: Ground electronic states and Energy gap engineering // J.Phys.Chem. A 2008, **112**, 12677.
78. *Stein S.E., Brown R.L.* pi.-Electron properties of large condensed polyaromatic hydrocarbons // J.Am.Chem.Soc. 1987, **109**, 3721.
79. *Fujita M., Wakabayashi K., Nakada K., Kusakabe K.* // Phys.Soc.Jpn. 1996, **65**, 1920.
80. *Nakada K., Fujita M., Dresselhaus G., Dresselhaus M.S.* Edge state in graphene ribbons: Nanometer size effect and edge shape dependence // Phys.Rev. 1996, **54B**, 17954.

81. *Miyamoto Y., Nakada K., Fujita M.* First-principles study of edge states of H-terminated graphitic ribbons // Phys.Rev. 1999, **59B**, 9858.
82. *Kobayashi Y., Fukui K., Enoki T., Kusakabe K., Kaburagi Y.* Observation of zigzag and armchair edges of graphite using scanning tunneling microscopy and spectroscopy // Phys.Rev. B. 2005, **71**, 193406.
83. *Niimi Y., Matsui T., Kambara H., Tagami K., Tsukada M., Fukuyama H.* Scanning tunneling microscopy and spectroscopy of the electronic local density of states of graphite surfaces near monoatomic step edges // Phys.Rev. B 2006, **73**, 085421.
84. *Jiang D., Sumper B.G., Dai S.* Unique chemical reactivity of a graphene nanoribbon's zigzag edge, // J.Chem.Phys. 2007, **126,** 134701.
85. *Lee H., Son Y-W, Park N, Han S., Yu J.* Magnetic ordering of graphitic fragments: Magnetic tail interaction between the edge-localized states // Phys.Rev. 2005, **72B**, 174431.
86. *Jiang D., Sumper B.G., Dai S.* First principles study of magnetism in nanographenes // J.Chem.Phys. 2007, **127**, 124703.
87. *Hod O., Barone V., Scuseria G.E.* Half-metallic graphene nanodots: A comprehensive first-principles theoretical study // Phys. Rev. B 2008, **77**, 035411.
88. *Dutta S., Lakshmi S., Pati S.K.* Electron-electron interaction on the edge states of graphene: A many-body configuration interaction study // Phys. Rev. 2008, **77B**, 073412.
89. *Meyer J.C., Girit C.O., Crommie N.F., Zettl A.* Imaging and dynamics of light atoms and molecules on graphene // Nature 2008, **454**, 319.
90. *Ph., Nayak S. K.* Electronic structure and band-gap modulation of graphene via substrate surface chemistry // Appl. Phys. Lett. 2009, **94**, 032101.
91. *Elias D.C., Nair R.R., Mohiuddin T.M.G., Morozov S.V. , Blake P., Halsall M.P., Ferrari A.C., Boukhvalov D.W., Katsnelson M.I., Geim A.K., Novoselov K.S.* Control of Graphene's Properties by Reversible Hydrogenation: Evidence for Graphane // Science 2009, **323**, 610.
92. *Hachmann J., Dorando J.J., Aviles M., Chan G.K.* The radical character of the acenes: A density matrix renormalization group study // J.Chem.Phys. 2007, **127**, 134309.
93. *Poater J., Bofill J.M., Alemany P., Sola M.* Local Aromaticity of the lowest-lying Singlet states of [*n*]acenes (*n*) 6-9) // J.Phys.Chem. 2005, **109A**, 10629.
94. *Sheka E.F., Chernozatonskii L.A., Artyukh A. A.* Graphene nanotube structures: Constitution and formation energy // JETP Letters 2009, **89**, 352.
95. NT08 Ninth International Conference on the Science and Application of Nanotube // Le Corum, Monpellier, France, June 29th-July 4th, 2008.
96. *Son Y-W., Cohen M.L., Louie S.G.* Half-metallic graphene nanoribbons // Nature 2006, **444**, 347.
97. *Van Fleck J.H.* The Theory of Electric and Magnetic Susceptibilities // Oxford, 1932.
98. *Shibayama Y., Sato H., Enoki T., Endo M.* Disordered magnetism at the metal-insulator threshold in nanographite-based carbon materials // Phys. Rev. Lett. 2000, **84**, 1744.
99. *Enoki T., Kobayashi Y.* Magnetic nanographite: an approach to molecular magnetism // J.Mat.Chem. 2005, **15**, 3999.
100. *Geim A.K., Novoselov K.S.* The rise of graphene // Nature Materials 2007, **6**, 183.
101. *Kara A., Leandri C., Davila M.E., de Padova P., Ealet B., Ougaddou H., AufrayB., Le Lay G.* Physics of silicene stripes // 2008, arXiv:0811.2611v1., http//arXiv.org/0811.2611v1.
102. *Sheka E.F.* May silicone exist? // 2009, arXiv:0901.3663v1, http://arXiv.org/abs/0901.3663 23 Jan 2009.
103. *Guzman-Verri G.G., Lew Yan Voon L.C.* Electronic structure of silicon-based nanostructures // Phys.Rev. 2007, **76B**, 075131.
104. *Fagan S.B., Baierle R.J., Mota R., da Silva A.J.R., Fazzio A.* Ab initio calculations for a hypothetical material: Silicon nanotubes // Phys.Rev. 2000, **61B**, 9994.
105. *Zhang R.Q., Lee S.T., LawC.-K., Li W.-K., Teo B.K.* Silicon nanotubes: Why not? // Chem.Phys.Let. 2002, **364**, 251.
106. *Yan B., ZhouG., Wu J., Duan W., Gu B.-L.* Bonding modes and electronic properties of single-crystalline silicon nanotubes // Phys.Rev. 2006, **73B**, 155432.
107. *Perepichka D., Rosei F.* Silicon nanotubes // Small 2006, **2**, 22.
108. *de Padova P., Quaresima C., Perfetti P., Olivieri B., Leandri M.E., Aufray B., Vizzini S., Le Lay G.* Growth of straight, atomically perfect, highly metallic silicon nanowires with chiral asymmetry // Nano Lett. 2008, **8**, 271.
109. *Gaspar P., Herold B.J.* Silicon, germanium, and tin structural analogues // In Carbene Chemistry, 2nd edn., Ed. W.Kirsme Academic Press, New York , 1971, 13, 504.
110. *Sheka E.F.* Violation of covalent bonding in fullerenes // In Lecture Notes in Computer Science, Computational Science – ICCS2003, Eds. Sloot P.M.A., Abramson D., Bogdanov A.V., Dongarra J., Zomaya A.Y., Gorbachev Y.E., Springer : Berlin, Part II, 2003, 386-398.
111. *Bao-xingL., Pei-lin C., Duan-lin Q.* Distorted icosahedral cage structure of $Si_{60}$ clusters // Phys.Rev. B 2000, **61**, 1685.
112. *Chen Z., Jiao, H., Seifert, G., Horn A.H.C., Y, D., Clark T., Thiel W., von Rague Schleyer P.* The structure and stability of Si60 and Ge60 cages: A computational study // J. Compt. Chem. 2003, **24**, 948.